Toward Direct Thermal-to-Electric Conversion: On-chip Microreactors for Catalytic Combustion of Methanol-Air Mixture

by
Sheng Tian

A thesis submitted in partial fulfillment of the requirements for the degree of

Master of Science
in
Chemical Engineering

Department of Chemical and Materials Engineering
University of Alberta

Abstract

In this thesis, on-chip microreactors for catalytic combustion of methanol-air mixture were designed, fabricated and characterized. Using standard optical lithography, deep reactive-ion etching (DRIE) and other fabrication techniques, microreactors with integrated micropillars having four different types of designs, viz., square and staggered pillar arrangements along with axial and diagonal flow configurations were generated. The diameter and height of the micropillars are both 100 μm and the available internal surface area of the reactor is 629.77 mm^2. Such microfabricated microreactors have a high surface-area-to-volume-ratio in the order of 27.80 mm^{-1}. A wash-coating procedure was adopted to deposit Pt on Al_2O_3 catalyst onto the reactor surfaces. After a preheating procedure, by introducing methanol-air mixture into the reactors, an autonomous and stable on-chip catalytic combustion could be sustained. This work shows that apart from the catalyst, fuel type, fuel and air flow rates, the geometric configuration of the microreactor plays a significant role in terms of achieving highest on-chip temperature. It was found that the on-chip microreactor with squared pillar arrangement coupled with diagonal flow configuration provided the best performance for the catalytic combustion of methanol-air mixture. It was also demonstrated that the well-known transition from heterogeneous catalytic combustion to a mixed heterogeneous-catalytic-and-homogeneous-gas-phase combustion exists during the combustion process in these on-chip microreactors. Such sustained catalytic combustion can be utilized as future heat source for direct thermal-to-electric energy conversion platform where the

on-chip microreactors can be packaged with commercial thermoelectric modules to achieve power generation on-chip.

Preface

Part of Chapter 2 and Chapter 3 has been submitted for publication in *Energy & Fuels*, May, 2014, *Under Review*, as Sheng Tian, Thomas Thundat, Kenneth C. Cadien, and Sushanta K. Mitra, "On-chip Catalytic Combustion of Methanol-Air Mixture". I was responsible for all the experiments performed, data collection and analysis, as well as the manuscript composition. Dr. Mitra and Dr. Thundat were the supervisory authors as well as co-PI of the Nano-Catalytic Energy Cell project, Dr. Cadien was the PI, they were all involved with results discussion and manuscript composition.

Section 2.3.1, Section 4.1 and Section A-2 of this thesis were published as Sheng Tian, Thomas Thundat, Subir Bhattacharjee, Kenneth C. Cadien, and Sushanta K. Mitra, "On-chip power generation: Microfluidic-based reactor for catalytic combustion of methanol", In ASME 2013 International Mechanical Engineering Congress and Exposition, pages V07BT08A005-V07BT08A005, American Society of Mechanical Engineers. I was responsible for experimental set-up designing and building, microreactor fabrication, all the experiments performed, data collection and analysis, as well as the manuscript composition. Dr. Mitra and Dr. Thundat were the supervisory authors as well as co-PI of the Nano-Catalytic Energy Cell project, Dr. Cadien was the PI and Dr. Bhattacharjee was co-PI. They were all involved with concept formation, results discussion and manuscript composition.

To My Parents and Yiwen

Acknowledgements

First of all, I would like to thank my supervisors, Dr. Sushanta Mitra and Dr. Thomas Thundat for their tremendous support and constant guidance for research during my two years M.Sc study. Dr. Mitra is one of the most hard-working people I have ever met in my life. All the emails coming at 6 am in the morning always remind me to keep working hard as what Dr. Mitra does. Also, his incredible ability to manage academic research, teaching, team personnel and international collaboration at the same time is quite impressive. I owe a great debt to him for all the time he spent with me discussing my project progress, revising my papers as well as presentations and even conducting experiments in the lab. Dr. Thundat is a world-class scientist whose expertise lies on nanomechanical systems, scanning probe microscopy and so on. It is my great honor to work with him and learn from him. On one hand, his solid and strong fundamental knowledge about physics, chemistry and biology is amazing, on the other hand, he never forgot to tell me to think about the practical application of our techniques and theories. I am deeply grateful to his encouragement and trust.

My heartfelt appreciation goes to Dr. Ken Cadien, who is the principal investigator of the Nano-Catalytic Energy Cell project I am working on. I thank him for providing this great opportunity in which I could enjoy doing research in such a interdisciplinary field and working with so many great talents in the past two years. Whenever I needed anything for my work or any advice for my career, Dr. Cadien was always there. Without his persistent help and support, my papers, conference presentation and this thesis would not have been possible.

I would like to thank the members of my examining committee: Dr. Neda Nazemifard (Chair) and Dr. Hyun-Joong Chung (Examiner-Arm's Length) for re-

viewing my thesis.

I am grateful to colleagues in Micro and Nano-scale Transport Laboratory (MNTL) and Nano Interfaces and Molecular Engineering Group (NIME) for their untiring support and help. It has been a great journey working with them. Special thanks to Dr. Naga Siva Kumar Gunda and Dr. Prashant R. Waghmare from MNTL for their insightful comments and suggestions to my project, to my study and life. I also want to thank Dibyo Sarkar, Anil Stephen, Arnab Guha, Aleksey Baldygin, Pankaj Sahu from MNTL and Dr. Xunchen Liu, Keren Jiang from NIME for all the good time we have gone through.

This thesis could not have been completed without a number of people. I received generous support and help from Nano-Catalytic Energy Cell teammates, Arash Baladi and Mengmeng Miao at numerous occasions. I have benefited a lot from staff members in Machine Shop, Mechanical Engineering and nanoFAB facility for building my experimental set-up and fabricating microreactor. A special mention goes to Roger Marchand from Machine Shop, Stephanie Bozic and Scottt Munro from nanofab. Dr Natalia Semagina (Department of Chemical and Materials Engineering, University of Alberta) gave me constructive comments and warm encouragement when I was searching an appropriate catalyst and deposition method. Discussions with her was illuminating.

I would also like to express my gratitude to Natural Sciences and Engineering Research Council (NSERC) of Canada for the financial support as Strategic Project Grants.

Last but most importantly, I thank my parents for their love and care I have extremely been indebted to, in all aspects, all the time.

Contents

List of Tables

List of Figures

Chapter 1

Introduction

1.1 Motivation and Background

"Portable Energy Gap" is getting larger, which is attributed to the phenomenon that the research development of conventional rechargeable batteries advances much slower compared with the rapid evolution of power-hungry electronic devices. As we can see nowadays, many high-tech companies are bringing more and more computing, entertainment and communication portable equipments that people couldn't live without, resulting in a ever-growing huge demand of power generating and supplying systems featured with higher energy density and longer operational life. In addition, along with strengthening of ecological protection awareness, people are expecting more environmental-friendly products. However, because of the toxic materials and heavy metals contained, discarded conventional batteries with their possible hazards are big threats to environment. Apparently, the further progress and applications of such batteries are seeing very significant bottlenecks, which forces scientists and researchers to turn their attentions to other power generation and energy conversion methods.

In the past few decades, massive efforts have been made to design and fabricate fuel cell systems (Dyer, 2002; Hibino et al., 2000; Murray et al., 1999; Park et al., 2000; Rostrup-Nielsen, 2001) based on hydrocarbons. Compared with the fact that people's current main choices of power source, for example rechargeable lithium batteries, are facing issues and challenges (Goodenough and Kim, 2009;

Tarascon and Armand, 2001), devices consuming hydrocarbon fuels possess lots of advantages in many different aspects, such as availability and portability. Regarding energy density, taking methanol for instance, the datum of which is about 19.7 MJ/kg, nearly 27 times higher than that of lithium-ion battery (0.72 MJ/kg). The higner energy density of fuel, the more chemical energy stored for further converting, which means power generators based on hydrocarbons may provide several orders of magnitude higher electrical power than conventional batteries of the same weight. Meanwhile, hydrocarbon-consuming fuel cell systems offer cleaner power generation and less greenhouse emissions, as they produce only water and CO_2. They also operate quietly and can be more efficient for energy conversion (Winter and Brodd, 2004).

Although the development of such fuel cell systems, like polymer electrolyte membrane fuel cell (PEMFC) (Ledjeff and Nolte, 1999; Smitha et al., 2005), direct methanol fuel cell (DMFC) (Arico et al., 2001; Wasmus and Küver, 1999) and solid oxide fuel cell (SOFC) (Ormerod, 2003; Park et al., 2000), is reaching the age of maturity, they still suffer from problems or challenges, such as great manufacturing costs (Winter and Brodd, 2004), poor performance of separation membrane (Mehta and Cooper, 2003), catalyst poisoning (especially CO from uncomplete reaction) (Gottesfeld and Pafford, 1988), and methanol cross-over (Gurau and Smotkin, 2002), etc.. These disadvantages restrict their further development, broader application and commercialization, making fuel cell systems less and less likely to become appropriate alternatives for conventional rechargeable batteries. New materials (Steele and Heinzel, 2001) and novel system design (Faghri and Guo, 2005) with better energy management are needed for serving superior performance of fuel cell.

Direct thermal-to-electric energy conversion is a novel method for power generation by using thermoelectric platform, the mechanism of which is on the basis of Seebeck effect, totally different from conventional batteries or fuel cell. In a typical thermoelectric power generation system, a heat source placed at the junc-

tion of two conducting materials with different Seebeck coefficient, one containing positive holes and the other negative electrons, would cause a current loop, that is electricity, from the temperature difference maintained between the hot and cold sides bridged by thermoelectrical materials in the middle. (DiSalvo, 1999) Devices based on thermoelectric phenomenon have the advantages of containing no moving parts, operating quietly, environmental friendly and relatively high energy density and conversion efficiency. These features make direct thermal-to-electric energy conversion utilizing thermoelectric effect a promising pathway to narrow the present "Portable Energy Gap" and meet people's demand for satisfying power generating and supplying systems.

Researchers are focusing on building catalytic combustors and using them as the potential heat sources for thermoelectric modules within the direct thermal-to-electric energy platform. S. B. Schaevitz et al. (Schaevitz et al., 2001) designed and fabricated a thermoelectic generator with integrated catalytic combustion of H_2-air mixture on membrane (Srinivasan et al., 1997). The platinum catalyst was deposited into the micromachined reactors. The heat generated by the combustion created a temperature gradient between thermopile junctions which could be further converted to electric power. The device can operate at the temperature as high as 500 °C with an output of voltage up to 7 V and a conversion efficiency up to 0.02%. K. Yoshida et al. (Yoshida et al., 2006) built a catalytic butane combustor with which they achieved complete combustion of butane over Platinum and a temperature of 300 °C. They bonded the combustor with 34 couples of BiTe thermoelectric elements and utilized such system to generate electric power based on catalytic combustion of H_2. They obtained a maximum output power of 184 mW and a total efficiency of 2.8%. Karim A. M. at al. (Karim et al., 2008) explored the catalytic combustion of methanol over Pt/Al_2O_3 in a microburner consisting of anodized alumina wafers, concluding that the combustion reaches steady stage with higher air flow rates and the mixing ratio of methanol to air hardly change the "start-up" time. They further integrated such microburner with thermoelectric module and achieved a maximum power generation as 0.65 W with a maximum thermal efficiency as

1.1%. Marton et al. (Marton et al., 2011) demonstrated the fabrication of rectangular half-channels with the dimension of 500 μm deep and 1050 μm wide on silicon wafer as well as the combustion of butane over an alumina-supported platinum catalyst. Integration with bismuth telluride thermoelectric modules to such system achieved a 5.82 W of electrical power with 2.53% efficiency, both of which are the highest reported in literature. S. Yadav et al. (Yadav et al., 2014) designed a prototype micro-thermoelectric power generator based on microcombustion of propane with the flow rate as 55 mLPM. The system successfully generated a voltage of 4.34 V and a current of 0.54 A with the maximum power as 2.35 W.

Recently, many studies have been reporting catalytic combustion of methanol over platinum-based catalyst. According to the work by Hu Z. et al. (Hu, 2007; Hu et al., 2005), such reaction taking place in a platinum-nanoparticles-supported quartz glass wool system within a glass tube can start from room temperature and present two different mechanism, a low temperature heterogeneous-only catalytic combustion and a high temperature combination of a heterogeneous catalytic and homogeneous gas-phase combustion. D. Resnika et al. (Resnik et al., 2012) built a catalytic microcombustor for methanol-air over Pt/CeO_2 synthesized based on micromachining of Si. After the initial pre-heating process to start the reaction, an autonomous and stable catalytic combustion of methanol-air was sustained. A temperature higher than 300 °C was obtained. Y. Ma. et al. (Ma et al., 2008) compared the performance of catalytic methanol combustion over dispersed platinum nanoparticles for different catalyst size, loading and flow residence time in a quartz flow reactor. J. R. Applegate et al. fabricated platinum nanoparticles with a colloidal synthesis technique (Applegate et al., 2012) and further tested them in an extruded cordierite monolith as the reactor. (Applegate et al., 2013) It was found that such catalyst could sustain the combustion of methanol from room temperature. They also showed an overall methanol conversion rate as high as 60%. via gas chromatography (GC). W. Yuan. et al. (Yuan et al., 2014) focused on designing a methanol combustor with $Pt\text{-}Al_2O_3$ catalyst dispersed on nickel (Ni) foam. They recommended higher loading of catalyst for lower ignition temperature and

proposed to optimize Al_2O_3 sol in order to improve catalyst dispersion and performance.

In this work, we report a novel way to create promising heat sources for thermoelectric modules and direct thermal-to-electric energy conversion systems. By using standard optical lithography, reactive-ion etching (RIE) and other fabrication techniques, on-chip microreactors with integrated micropillars for catalytic combustion of methanol-air mixture were fabricated. Such reactors can be easily integrated with thermoelectric apparatus to achieve power generation on-chip.

1.2 Objective

The objective of the this thesis is to develop on-chip microreactors for sustaining catalytic combustion of methanol-air mixture which can be utilized as future heat source for direct thermal-to-electric energy conversion platform.

This work involves design and fabrication of on-chip microreactors, detailed catalytic combustion characteristics, appropriate experimental apparatus building and further integration with commercial thermoelectric module.

1.3 Structure of This Thesis

The guidelines from the Faculty of Graduate Studies and Research (FGSR) at the University of Alberta have been followed to prepare the thesis and this thesis is arranged into the following five chapters with an appendix:

- Firstly, the Chapter 1 presents the motivation, background and objective of this work.
- Chapter 2 shows the details of the design, fabrication and catalyst deposition methods used of the on-chip microreactors proposed. Microfabrication techniques, characterizations of the microreactor and the Pt on Al_2O_3 catalyst are presented.

- Chapter 3 is about the entire experimental set-up and on-chip catalytic combustion characteristics. The results of chip temperature trace with time for different designs of microreactors are discussed and summarized.

- Chapter 4 shows the possibility of on-chip catalytic microreacotrs integrated with commercial thermoelectric module for direct thermal-to-electric conversion. The design of electric system and the experimental apparatus are introduced.

- Chapter 5 summarizes the key conclusions and results of this research. Future prospects based on the outcome of this work for further study and improvement of the project are also recommended.

- The Appendix part includes the detailed fabrication techniques used, preliminary fabrication results and raw data analysis.

Chapter 2

Development of On-chip Microreactors: Design, Fabrication and Catalyst Deposition[1]

2.1 Microreactor Design Background

Recent trends in miniaturization of chemical systems, such as reactors for synthesis of organics (Mason et al., 2007) or nanomaterials (Wagner and Köhler, 2005), microactuators for pumps (Tanaka et al., 2006) or valves (Low et al., 2000), micromixers (Hessel et al., 2005) and microseparators (Han and Frazier, 2006), have opened up new opportunities to perform complex reactions in microfluidic chips (Beebe et al., 2002; Jähnisch et al., 2004; Jensen, 2001). Performing reaction on-chip provides significant enhancement in terms of increased heat and mass transfer resulting from high surface-area-to-volume ratio. Advancements in micro/nanofabrication have also enabled researchers to fabricate complex geometrical configurations, like pillars (Gunda et al., 2013a) and wells (Gunda et al., 2013b), integrated within the microchannels, which have further created tremendous potential to test different on-chip chemical or biological reactions, for example, digital polymerase chain reaction (Men et al., 2012), detection of dengue NS1 virus (Gunda et al., 2013c) and even catalytic combustion of methanol (Tian et al., 2013), etc.

[1]Part of this chapter has been submitted for publication, *Energy & Fuels*, May, 2014, *Under Review*. Sheng Tian, Thomas Thundat, Kenneth C. Cadien, and Sushanta K. Mitra

One of the most commonly studied chemical reactions is the combustion of hydrocarbons, like methanol in air (Hucknall, 1985). Catalytic oxidation of methanol vapor over metallic platinum was reported for the first time by J. G. Firth (Firth, 1971), where a complete reaction to carbon dioxide and water with excess oxygen was performed. More recently, Hu et al. (Hu et al., 2005) have demonstrated that the use of platinum nanoparticles can sustain the combustion of methanol-air mixture starting at ambient temperature, where the combustion temperature obtained was as high as 600 °C. In their work, Pt nanoparticles loaded quartz glass fibers were used to create the combustion substrate and they showed different regimes for reaction rates, viz., heterogeneous catalytic reaction; gas-phase ignition; and steady self-supporting combustion. More importantly, these regimes were found to be a function of the fuel/air ratio and gas flow rate. Therefore, it is interesting to find out whether such commonly performed catalytic combustion in a macro-system can be achieved in a microsystem to take advantage of enhanced surface-area-to-volume ratio.

Norton et al. (Norton et al., 2006) designed and manufactured catalytic microreactors for combustion of C_3H_8 and H_2 with stainless steel (SS) casing and studied the thermal management of such combustors both experimentally and by CFD simulations. They found that the performance of such catalytic reaction is affected by heat and mass transfer issues. Federici et al. (Federici et al., 2006) further tested the catalytic combustion of C_3H_8/air and H_2/air on platinum catalyst with the same configuration as the one reported by Norton et al. (Norton et al., 2006). They achieved complete combustion over a range of flow rates and an uniform temperature about 300°C with the help of thermal spreader. Karim et al. (Karim et al., 2008) have also studied the catalytic combustion of air/methanol inside a similar rectangular microburner of dimension 1 cm wide by 6 cm long and they used platinum supported on anodized alumina as a substrate inside the microburner. They achieved a combustion temperature in excess of 600 °C and showed that the combustion start-up time is a strong function of the air flow rate. Applegate et al. (Applegate et al., 2013) used a different configuration of microreactor for catalytic combustion

of methanol, which is based on a bundle of cylinders (each 800 μm channel width) in an extruded cordierite monolith. They introduced platinum nanoparticles with a draw coating technique and achieved a much higher combustion temperature close to 850 °C.

Marton et al. (Marton et al., 2011) demonstrated that one can further miniaturize a reactor by using microfabrication techniques, where they fabricated rectangular half-channels of dimension 500 μm deep and 1050 μm wide on silicon wafer and performed the combustion of butane over an alumina-supported platinum catalyst. Resnik et al. (Resnik et al., 2012) have also used silicon microfabrication techniques to build their microreactor comprising of inlet and outlet microchannels (600 μm wide and 140 μm deep) for methanol/air delivery and product exhaust, respectively, while the combustion chamber was directly etched on a silicon wafer up to a depth of 140 μm with an available reaction area of 350 mm^2. Using Pt/CeO_2 catalyst, they obtained stable combustion at temperatures over 300 °C and showed the presence of different combustion regimes based on different reaction rates, as demonstrated by Hu et al. (Hu et al., 2005). Also, they required a pre-heating of at least 100 °C (referred as light-off temperature) to start the combustion of methanol-air (O_2) fuel feed.

Existing literature suggest that the use of microfabrication techniques to generate large surface area combustion chamber is still an evolving area of research, where there is a significant opportunity to introduce patterned substrate integrated within the microchannel reactor area to further enhance combustion efficiencies. In this chapter, we have demonstrated the use of micropillar integrated microchannel configuration as an on-chip reactor to achieve catalytic combustion of methanol-air mixture. The catalyst in this case is Pt on Al_2O_3, deposited on the micropillar surfaces using wash-coating technique (Marton et al., 2011). We used two different micropillar arrangements, viz., squared and staggered, and for each arrangement, we applied two different flow configurations, viz., axial (i.e., pillars are aligned with the flow direction) and diagonal (i.e., pillars are at 45° to the flow direction).

We found that the combination of pillar arrangement and flow configuration plays a significant role on the performance of on-chip microreactors.

2.2 Fabrication of On-Chip Microreactors

Using standard optical lithography and reactive-ion etching (RIE) technique, micropillar integrated microchannels were generated on silicon wafers. The microfabrication procedure is illustrated in Figure 2.1, the details of which can be found elsewhere (Gunda et al., 2013a,c; Tian et al., 2013). The photo mask with four different designs to accommodate different pillar arrangements and flow configurations were designed with L-Edit (Tanner EDA Inc., USA). Each design consists of microfluidic ports, inlet and outlet flow regions and an array of 75 $\times$ 75 micropillars distributed within an area of 15 mm $\times$ 15 mm.

A $\sim$500 nm SiO_2 layer coated 4-inch-diameter Si wafer (purchased from nanoFab, University of Alberta) was first immersed in a standard Piranha solution (H_2SO_4 : H_2O_2 = 3 : 1) for about 15 min and dried with SpinRinseDryer. The wafer was then placed in YES HMDS Oven (Yield Engineering Systems, Inc., USA) for a full cycle. HDMS (hexamethyldisilazane) deposited on top of the substrate would assist adhesion of photoresist to SiO_2 layer. Next step was spin-coating of the positive photoresist (PPR) HPR 506 (Fuji-film Electronic Materials, Inc., USA) onto the silicon substrate using parameters as: (1) Spreading: 500 RPM for 10 s; and (2) Spinning: 4000 RPM for 40 s. Post bake was done using Solitec vacuum hotplate (Solitec Wafer Processing, Inc., USA) at 115 $^\circ$C for 90 s before transferring the integrated micropillar patterns onto the coated PPR layer, as the Si substrate was exposed to Ultraviolet (UV) light on ABM Mask Aligner (ABM, Inc., USA). After development of UV-exposed PPR, the non-PPR-covered SiO_2 layer was etched using STS RIE for 2 min 30 s. Isotropic etching of Si substrate for $\sim$100 μm using Bosch deep reactive-ion etching (DRIE) method was then conducted in STS ICP-RIE system. The Bosch process was alternated repeatedly between plasma etching and passivation layer deposition, until the pre-set number of etching cycles was

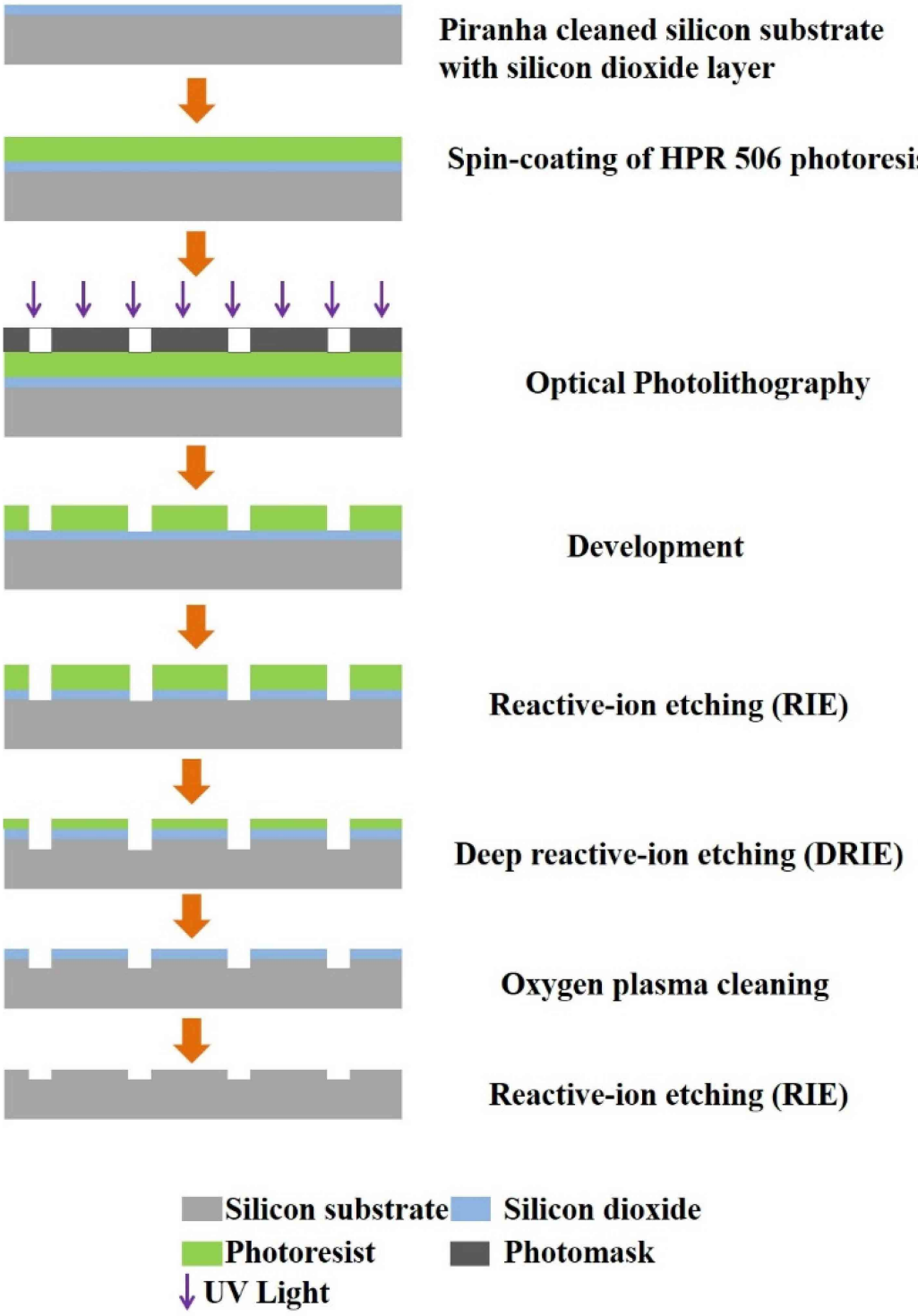

Figure 2.1: Schematic of the microfabrication process involved in obtaining micropillars on silicon wafer.

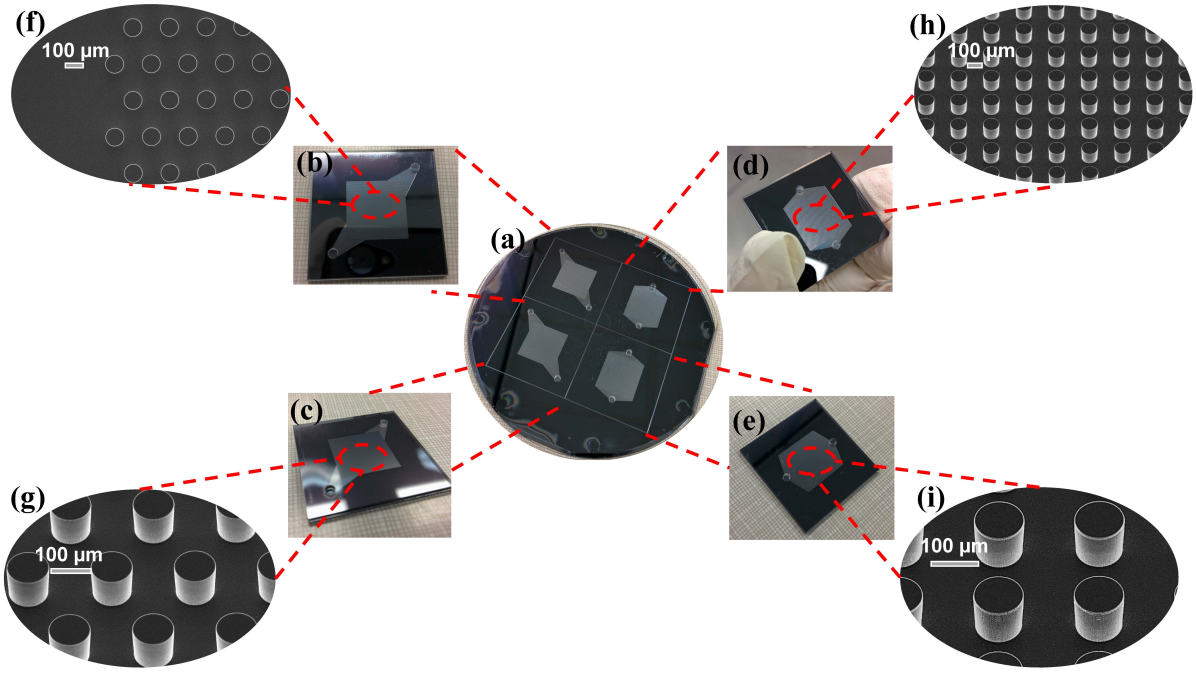

Figure 2.2: (a) Micropillar integrated microchannels on Si substrate bonded with borofloat glass cover on top. (b-e) On-chip microreactors with different pillar arrangements (squared, staggered) and different flow configurations (axial, diagonal). (f-i) SEM images of micropillars generated on Si substrate. The pillar diameter and height are both 100 µm. The interspacing distances for squared arrangement are 200 µm and for staggered arrangement are 223.6 µm and 200 µm.

reached. Due to the selectivity of the etching systems, PPR was also etched during this process. The SiO_2 layer underneath was thoroughly removed by STS RIE system after the residual thin PPR layer was cleaned by oxygen plasma in Branson Barrel etcher. Scanning electron microscope (SEM, LEO 1430, ZEISS, Germany) images of the generated micropillars on silicon substrate with different pillar arrangements (squared, staggered) are shown in Figures. 2.2 (f), (g), (h), and (i). The resulted pillar height and diameter are both 100 µm, with interspacing distances for squared arrangement as 200 µm (Figure 2.2 (i)) and for staggered arrangement as 223.6 µm and 200 µm(Figure 2.2 (g)).

Finally, the microfabricated chip needs to be closed to ensure proper fuel-air mixture delivery into the microreactor. Therefore, a 4-inch-diameter round borofloat glass drilled with inlet and outlet holes by abrasive water-jet cutter (2652 Jet Machining Center, USA) was bonded onto the micropillar integrated Si substrate using SUSS bonder (SÜSS MiroTec AG, Germany). An anodic bonding recipe applying high temperature and high pressure was used for this packaging purpose. The resulting borofloat glass covered Si wafer, shown in Figure 2.2 (a), was diced into four pieces representing the four desired designs by dicing saw (Diamond Touch). Hence, four on-chip microreactors were successfully fabricated, as shown in Figure 2.2 (b), (c), (d), and (e). All of these microreactors with the dimension of 32 mm $\times$ 32 mm and thickness of 1.6 mm have the same internal surface area as 629.77 mm^2, internal volume as 22.65 mm^3 and the surface-area-to-volume-ratio as 27.80 mm^{-1}.

2.3 Catalyst Deposition

2.3.1 Surface-selective Infiltration Method[2]

For preliminary experiments, we adopted a surface-selective infiltration method similar to (Chen et al., 2005) for catalyst deposition before the bonding procedure. Compared to other conventional coating procedures (Meille, 2006), such method would not only keep the reactor top surface clean for subsequent sealing via anodic bonding, but also precisely control the loading amount of catalyst. But this method which is based on liquid drop (with solid particles inside) deposition still suffer from the well-known coffee ring effect (Deegan et al., 1997), which tremendously decreases the uniformity and dispersion of catalyst deposited.

An hydrophobic Parafilm sealing film (American National Can Co., USA) was pressed onto the integrated micropillar area of the silicon wafer. By heating the

[2]A version of this section has been published in *ASME 2013 International Mechanical Engineering Congress and Exposition*, November, 2014, Sheng Tian, Thomas Thundat, Subir Bhattacharjee, Kenneth C. Cadien, and Sushanta K. Mitra, (pp. V07BT08A005-V07BT08A005), American Society of Mechanical Engineers.

wafer on a hot plate at 80°C for 10 min, the hydrophobic film became soft gradually. After peeling off, a residual layer of the Parafilm still remained on top of the area. As the Platinum (Pt) nanoparticles (NPs) are stabilized in a water-based suspension, they will therefore selectively coat only the inner surface of the silicon wafer but not the top surface. The Parafilm sealing film can be easily removed during the calcination later.

Pt NPs stabilized by polyacrylate sodium in a water-based suspension were purchased from Sciventions Inc., Canada, the concentration of which is 1.5 mg/ml. Particle size less than 10nm is observed from transmission electron microscopy (TEM). The surface of the silicon wafer with integrated micropillars is superhydrophobic, as the contact angle of Pt suspension droplet on it measured by Krüss Drop Shape Analysis System DSA100 (KRÜSS GmbH., Germany) is more than 145°. In order to increase the wettability of Pt suspension on the surface of Si substrate, same volume of absolute ethyl alcohol (SIGMA-ALDRICH Inc., USA) was added into the original suspension, as the surface tension of ethanol is much smaller. After mixing by a Vortex Mixer (Fisher Scientific, Canada) for 15 min, a certain volume of the water-ethanol-based Pt NPs suspension was measured by a micropipette. After injecting the Pt NPs suspension onto the Si substrate, the liquid would fill into the space between those micropillars quite rapidly. The contact angle of water-ethanol-based Pt suspension droplet was reduced to $\sim 40°$. As the top surface of the Si substrate remained hydrophobic during the drying of the catalyst, more cycles of Pt NPs deposition can be done, so that more amount of catalyst will be loaded into the reactor.

A model having square pillar arrangements along with axial flow configuration noted as 30_SQ_AX was chosen for characterization of catalyst deposition with surface-selective infiltration method. After 16 µl of water-ethanol-based Pt NPs suspension drop was injected onto the top surface using a micropipette, 30_SQ_AX was dried in the air overnight. The addition of ethanol can increase the wettability of the Pt suspension on superhydrophobic micropillar-patterned silicon substrate sig-

nificantly, which allows the fluid to fill into the region between micropillars within a few minutes. The resulting sample was characterized by SEM. From Figure 2.3 (a), we observed that after drying in the air, a pattern of dendritic structure was formed around the micropillars. The presence of polyacrylate sodium crystals was confirmed by energy-dispersive X-ray spectroscopy (EDXS). In some particular area, those crystals aggregate, forming thin film structure. Such morphology is not good for catalytic reaction, since the surface area of Pt NPs is covered tremendously. As a result, the active sites of Pt NPs for catalytic reaction are blocked. In order to smash the polyacrylate sodium crystal structure for increasing the catalytic activity, calcination was done by putting the sample of 30_SQ_AX in a furnace at 500°C for 150 min. Figs. 2.3 (c) and (d) show the top view of the resulting sample after calcination, during which process polyacrylate sodium was decomposed into sodium carbonate. Obviously, the morphology of crystal structure was changed into microsize particles making Pt NPs more accessible for catalytic reactants. EDXS mapping was done to confirm the distribution of Pt NPs. It was also observed that the hydrophobic Parafilm sealing film was removed during calcination, as top surface of Si substrate of the 30_SQ_AX sample became clean again afterward.

However, we also found that catalyst deposition with surface-selective infiltration method based on liquid drop deposition resulted in poor uniformity and bad distribution of catalyst particles, which would seriously influence the catalytic combustion performance. As shown in Figure 2.4, along the spill of the contact line of liquid drop after evaporation, millimeter-sized cluster of catalyst particles formed. Such phenomenon is attributed to the coffee ring effect, as a capillary flow within the evaporating drop pushes the particles from the centre to the edge (Deegan et al., 1997), leaving a stain-like structure along the perimeter of the dried liquid drop.

Obviously, unfavorable dispersion of catalyst particles is detrimental for catalytic reaction. Therefore, optimized catalyst deposition method should be explored. We tried a wash-coating technique after closed microreactors were fabricated which is discussed in the next section.

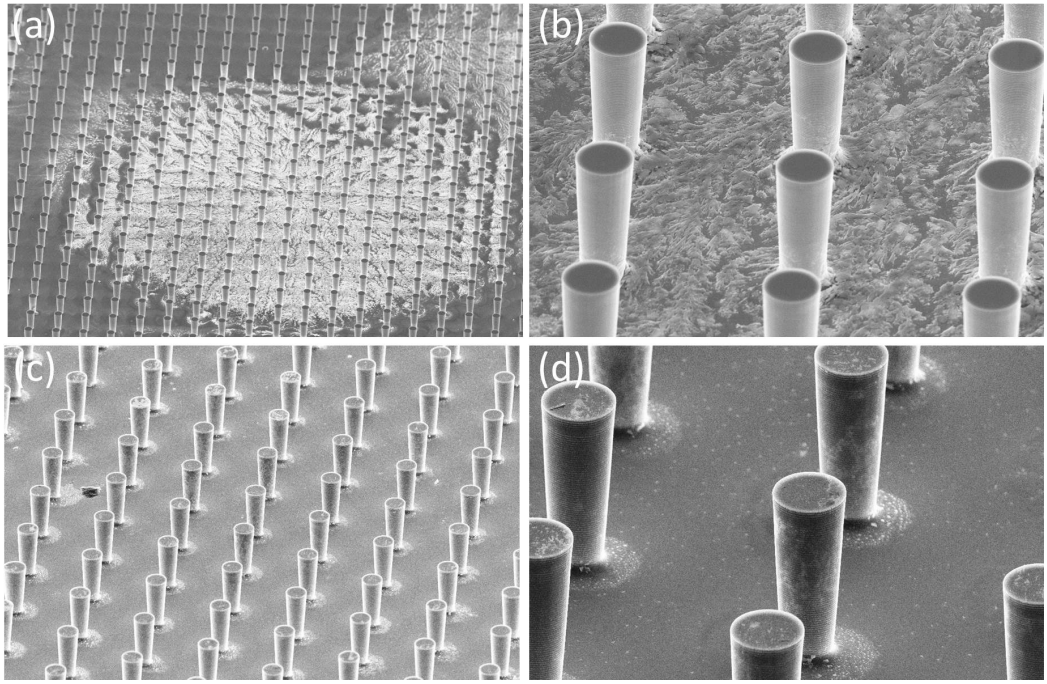

Figure 2.3: Morphology change of catalyst before and after calcination for 30_sq_ax. (a) Dendrite structure of polyacrylate sodium after drying. (b) Thin film structure of polyacrylate sodium after drying. (c) Morphology change of catalyst around pillars after calcination. (d) Magnified image of morphology change after calcination.

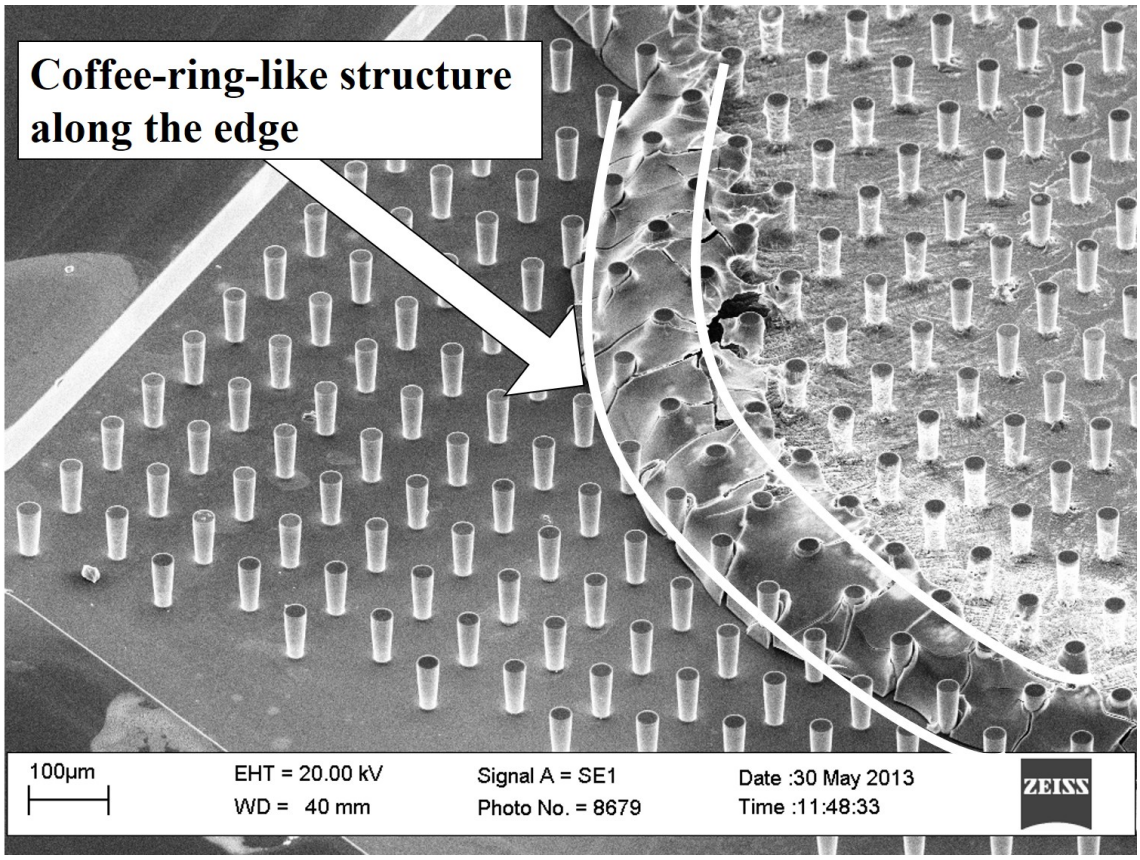

Figure 2.4: Cluster of catalyst particles formed along the perimeter of the contact line of liquid drop after evaporation because of the well-known coffee ring effect.

2.3.2 Wash-coating Technique

For catalyst deposition of all the reactors in on-chip catalytic combustion characterization experiments, a wash-coating procedure, similar to the one developed by Marton et al. (Marton et al., 2011), was used. The catalyst used here is 5% by weight Pt on Al_2O_3, purchased from Sigma Aldrich. After grinding catalyst particles in a mortar for about an hour, as shown in Figure 2.5 (a) and (b), we observed that big aggregates were dispersed, and the average size of the catalyst particles was reduced to only a few microns. Thus, platinum dispersion over alumina was increased enormously, resulting in a better catalytic activity. Then, a slurry prepared by mixing 1.5 g Pt/Al_2O_3 catalyst, 10 g deionized water and 150 µl colloidal nano-sized alumina binders gel was slowly and uniformly injected into the on-chip microreactor supported on a holder using a hand-operated syringe. The microreactors with squared pillar arrangement and axial flow configuration as well as staggered pillar arrangement and axial flow configuration after "washing" procedure are shown in Figure 2.6. As it shows, the washcoat of catalyst is evenly distributed onto all the silicon surfaces inside the reactors, which proves the adequate wettability of the water-based catalyst slurry. The reactor was first kept aside for about 15 min in order for the catalyst to get absorbed onto the silicon surface. The slurry residing in the space between the micropillars was then removed out by pressurized air and the reactor surface was cleaned properly. This step must be done before putting the reactor into a muffle furnace (Thermo Fisher Scientific, Inc., USA) for heating, otherwise the excess catalyst particles will block the microchannels, which eventually increases the pressure drop across the chip quite substantially. The heating temperature was set at 100°C for 25 min followed by 350 °C for 30 min, for drying and calcination process.

The mass of catalyst coated onto the microreactor was calculated by measuring the weight before and after the wash-coating procedure using a weight balance (Denver Instrument, USA). It was found that for all reactors, only $\sim$1.1 mg of Pt on Al_2O_3 catalyst, i.e., 0.55 µg of Pt was deposited. Thus, the loading of Pt nanopar-

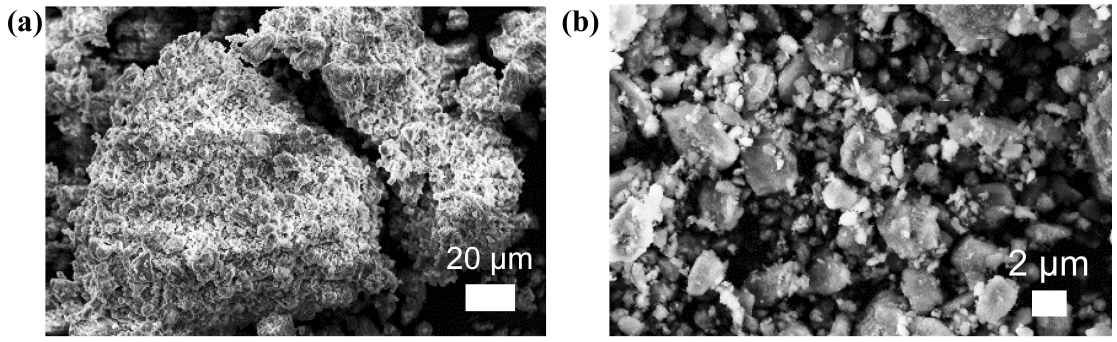

Figure 2.5: SEM images of Pt/Al_2O_3 particles (a) before grinding and (b) after grinding.

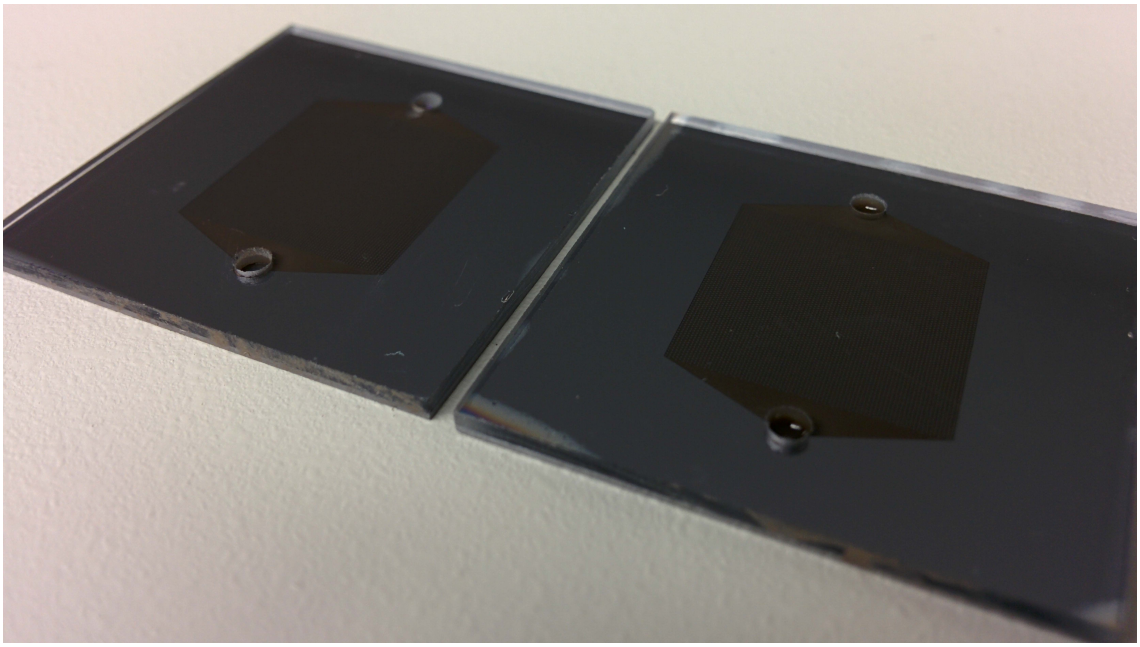

Figure 2.6: Microreactors with axial flow configuration after "washing" procedure.

ticles is $\sim$0.0087 mg/cm^2 of internal surface area for the on-chip microreactors.

Chapter 3

On-chip Catalytic Combustion Characterization: Results and Discussion[1]

3.1 Experimental Set-up and Chip-holder Design

The entire experimental set-up for the characterization of catalytic combustion is schematically depicted in Figure 3.1. It includes a chip-holder, whose exploded view is shown in Figure 3.1 (b) and the completely assembled chip, microfabricated by the process illustrated in Figure 2.1 and anodic packaging with further catalyst loading achieved through wash-coating procedure, as shown in Figure 3.1 (c). The assembled chip has one inlet port to connect with the methanol gas-wash bottle (500 ml, Sigma-Aldrich Co. LLC, USA), which holds the liquid methanol with traces of vapor phase present in the head space. We procured methanol from Fisher Scientific with 99.9% purity and poured the liquid inside this closed gas-wash bottle. In order to create appropriate fuel-air mixture, air is introduced into this gas-wash bottle from a compressed air cylinder (48.99 L, 80 psi, Praxair Canada, Inc., Canada), the flow rate of which is regulated using an in-line flowmeter (0-300 sccm, Praxair Canada, Inc., Canada). Also, the chip has one outlet port which is kept open to atmosphere and the exhausted gases are vented out using a fume hood.

[1]Part of this chapter has been submitted for publication, *Energy & Fuels*, May, 2014, *Under Review*. Sheng Tian, Thomas Thundat, Kenneth C. Cadien, and Sushanta K. Mitra

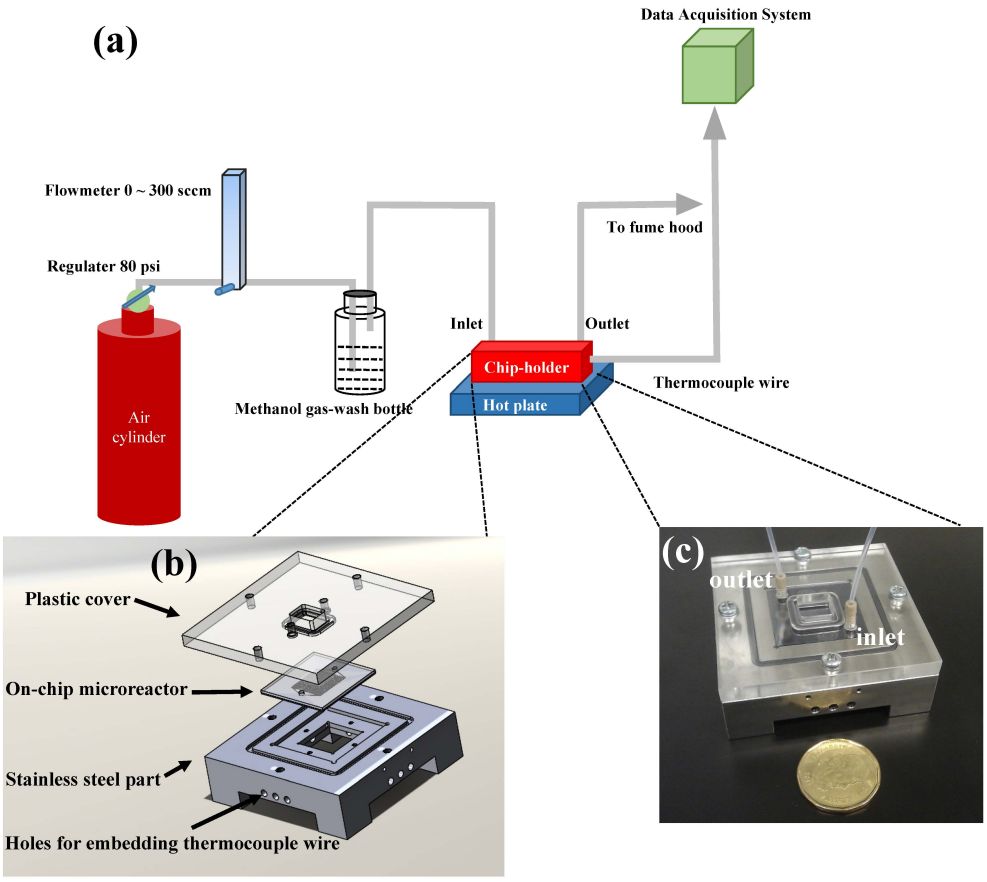

Figure 3.1: (a) Experimental set-up for characterizing the catalytic combustion of methanol-air mixture using microfabricated on-chip microreactor. (b) Exploded view of the chip-holder (plastic cover, stainless steel part) and on-chip microreactor. (c) Assembly of the chip-holder, on-chip microreactor and inlet/outlet ports.

In order to record the chip temperature, we have embedded a k-type thermocouple wire (McMaster-Carr Supply Company, USA), which is in contact with the bottom of the on-chip microreactor. This thermocouple wire is glued onto the silicon substrate using a piece of graphite thermal sheet (Custom Thermoelectric, Inc., USA) as shown in Figure 3.2. The other end of the thermocouple is connected to a data acquisition system (National Instruments Corporation, USA) and custom-built programming using LabVIEW has been incorporated to collect the required temperature data. During our combustion experiments, we need to maintain a light-off temperature, varying between 95 °C and 111 °C, which is achieved by placing a hot plate (120 V/60 Hz, 5-550 °C, Corning Incorporated, USA) underneath the chip holder.

3.2 On-chip Catalytic Combustion Results and discussion

Firstly, we observed that the catalytic combustion of methanol-air mixture over Pt on Al_2O_3 could not be achieved and sustained starting from the room temperature (23 °C). Hence, a preheating step must be provided. Therefore, for all subsequent combustion characterization experiments, we first put the chip-holder assembly on the hot plate to be heated up to a certain temperature (115 °C for microreactors with axial flow configuration and 95 °C for ones with diagonal flow configuration). Then the methanol-air mixture was introduced by turning on the valve of the flowmeter, which resulted in further increase of the chip temperature due to the start of the catalytic combustion. Once, the chip temperature, as recorded by the thermocouple wire with data acquisition system, reached a certain value (125 °C for microreactors with axial flow configuration and 110 °C for ones with diagonal flow configuration), the chip holder was removed from the hot plate. This causes a momentary reduction in the chip temperature. At this point, the methanol-air mixture was further supplied into the chip in order to prevent any extinction of the combustion process. The corresponding temperature is denoted as the light-off temperature and the corresponding air flow rate, as regulated by the flowmeter, is referred as the starting air

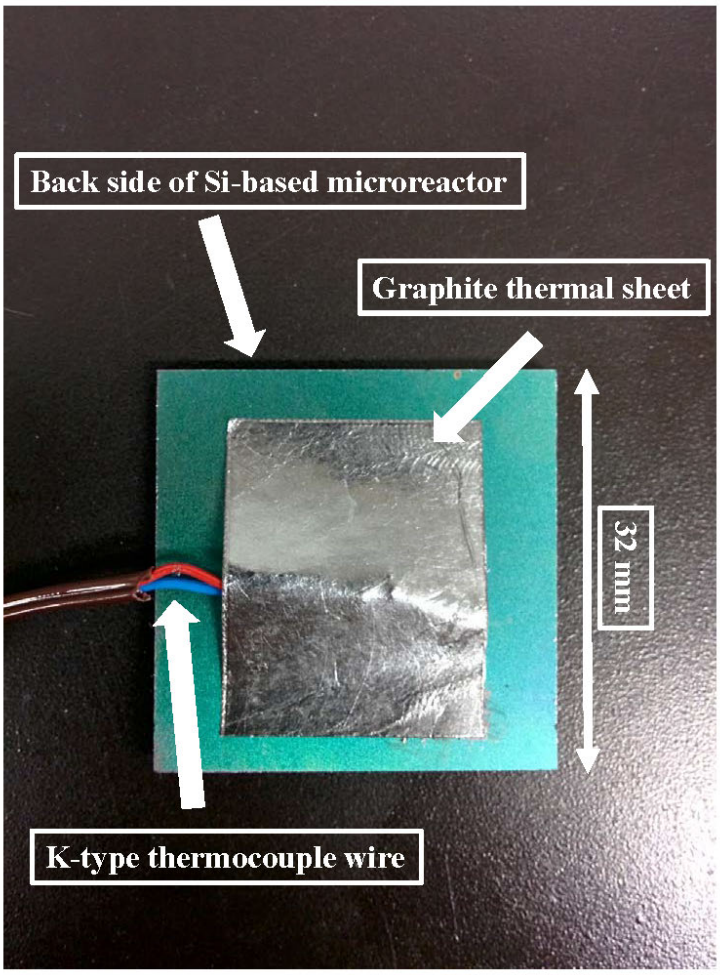

Figure 3.2: On the back side of the microreactor, the thermocouple wire is in contact with the silicon substrate with the help of a piece of graphite thermal sheet.

flow rate for all our experiments.

Figure 3.3 to Figure 3.6 show the combustion characteristics for four different designs of on-chip microreactors. In case of squared pillar arrangement with axial flow configuration, as described in Figure 3.3, the light-off temperature was 111 °C corresponding to the starting air flow rate of 207.39 sccm. The trace of the chip temperature over time can be divided into four key stages based on four different air flow rates, viz., 207.39 sccm, 249.47 sccm, 273.80 sccm and 0 sccm, respectively. It was observed that for this design, initially there was a dip in temperature during Stage I which was mitigated by increasing the flow rate. The maximum achieved temperature for this case was 115.9 °C. The inset plot in Figure 3.3 suggests that each time we increased the flow rate, there was a slight drop in temperature followed by the temperature rise. This was due to the fact that as the air flow rate increases, the methanol concentration decreases and consequently there is a corresponding increase in the velocity of methanol-air mixture (Ma et al., 2008), which breaks the balance between the heat generated and heat loss in a very short time period, causing a decrease in the temperature momentarily. Also, it was found that when we turned off the air flow (Figure 3.3 Stage IV), the temperature would drop immediately, which indicates the quick response of the catalytic reaction to the supplied methanol-air mixture. Similar observations were found for the cases of staggered pillar arrangement with axial flow configuration (Figure 3.4), squared pillar arrangement with diagonal flow configuration (Figure 3.5) and staggered pillar arrangement with diagonal flow configuration (Figure 3.6).

It is to be noted that for staggered pillar arrangement with axial flow configuration, as shown in Figure 3.4, we achieved a maximum temperate of 120.7 °C, which shows that this pillar arrangement allows adequate mixing of the fuel and air within the microreactor and most likely utilizes the catalyst efficiently as compared to the squared arrangement with a maximum temperate of 115.9 °C, as shown in Figure 3.3. It was also found that for diagonal flow configuration, as shown in Figure 3.5 and Figure 3.6, the maximum temperature achieved was 130.7 °C for

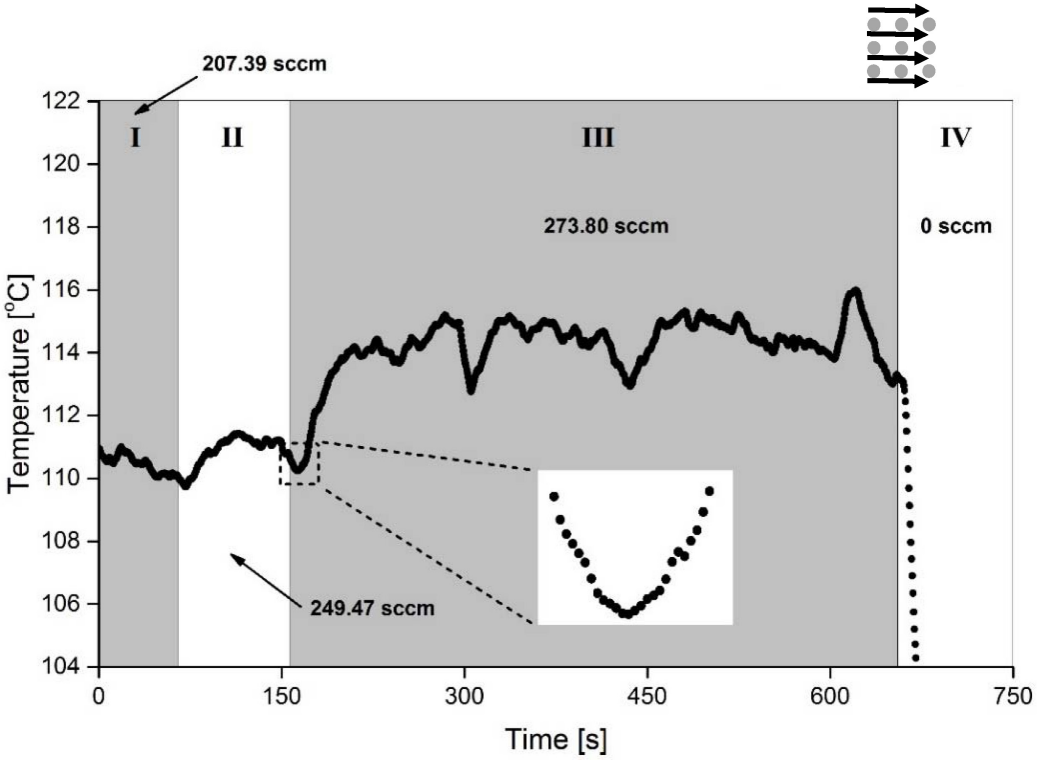

Figure 3.3: Temperature measurement of on-chip microreactor for squared pillar arrangement and axial flow configuration.

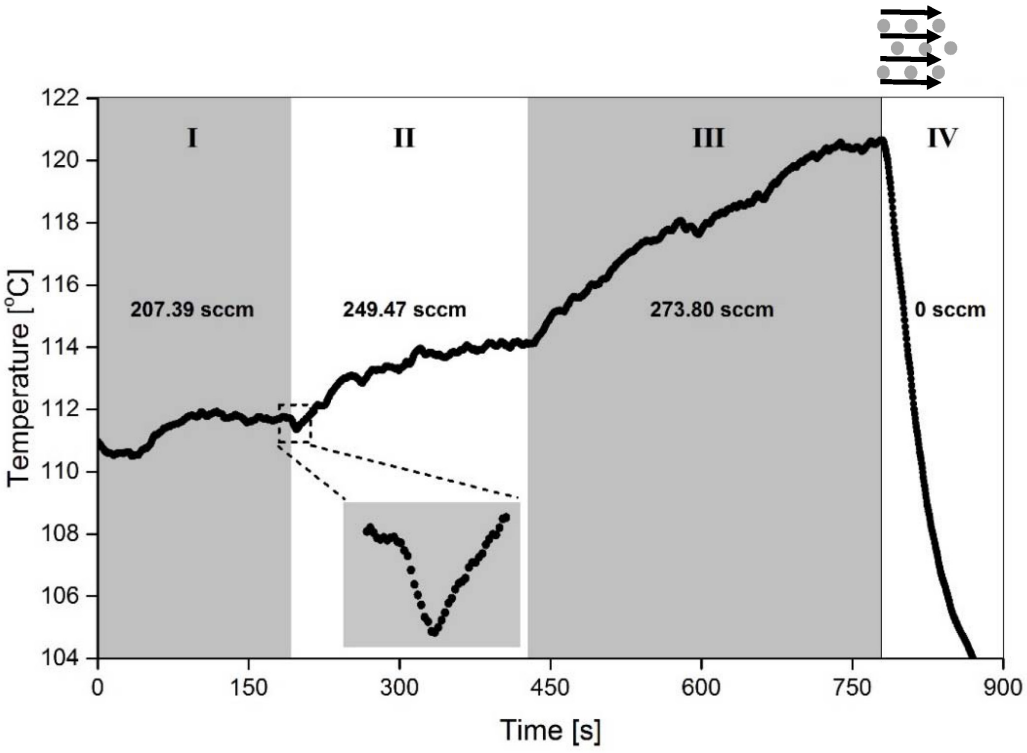

Figure 3.4: Temperature measurement of on-chip microreactor for staggered pillar arrangement and axial flow configuration.

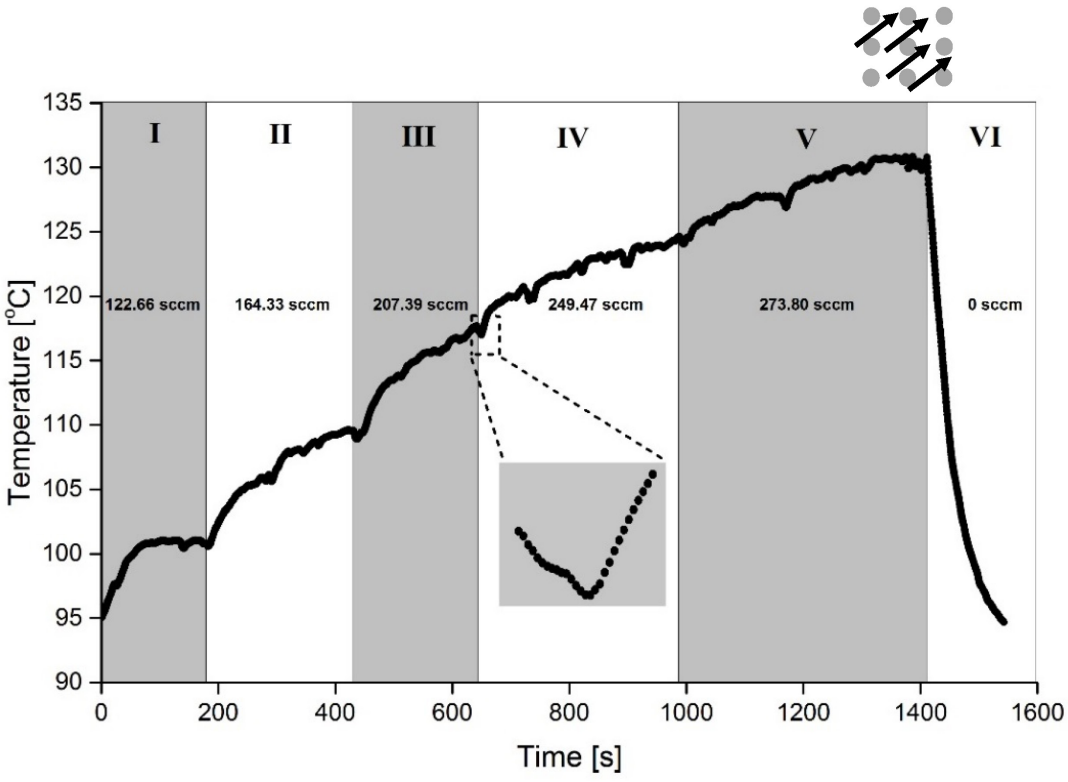

Figure 3.5: Temperature measurement of on-chip microreactor squared pillar arrangement and diagonal flow configuration.

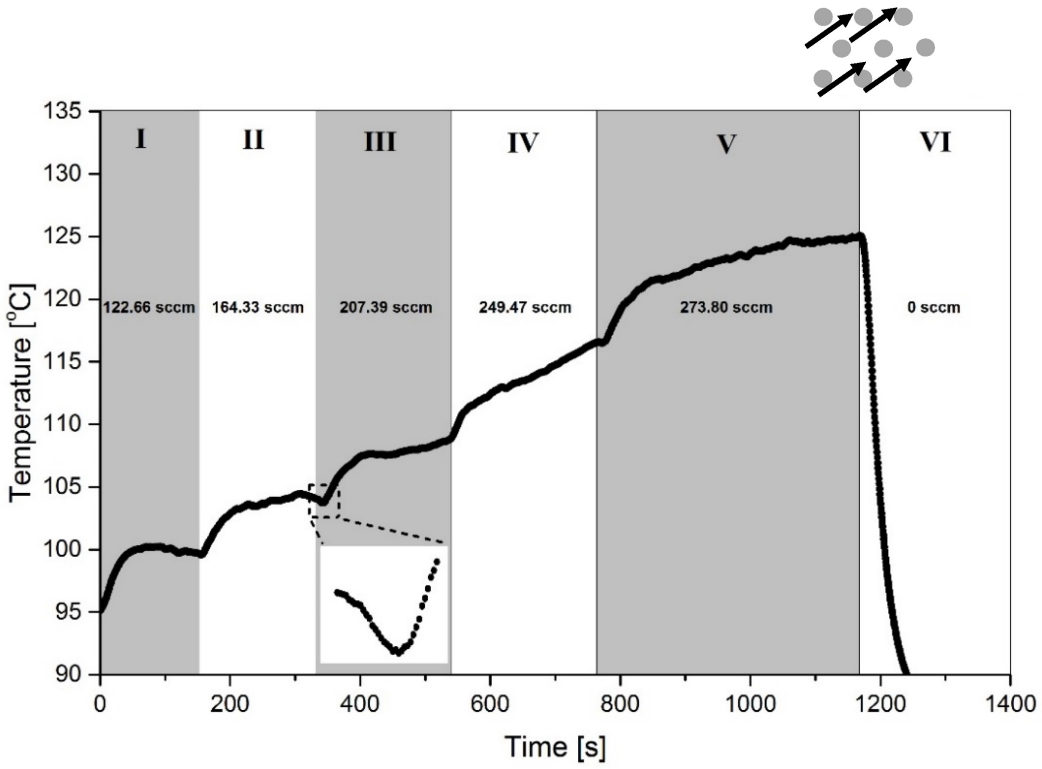

Figure 3.6: Temperature measurement of on-chip microreactor for staggered pillar arrangement and diagonal flow configuration.

squared pillar arrangement and 125.0 °C for staggered arrangement. This suggests that the diagonal flow with squared pillar arrangement creates favorable mixing as compared to the staggered arrangement, where the fuel-air mixture almost has parallel pathways to flow across the micropillars. One can argue that the configuration depicted in Figure 3.5, which provides opportunity for the fuel-air mixture to interact directly with the micropillars, is almost similar with Figure 3.4, where again the fuel-air is allowed to impinge on the pillars. Therefore, such configurations are advantageous for fuel-air mixture to get access to Pt on Al_2O_3 particles on the reactor surfaces.

There is a significant difference in the light-off temperature and starting air flow rate for microreactors with diagonal flow configuration as compared to the ones with axial flow configuration, viz., 95 °C and 122.66 sccm for diagonal flow configuration, while 111 °C and 207.39 sccm for axial ones. This can be attributed to the inlet flow geometry for the diagonal flow configuration, as shown in Figure. 3.7, where the inlet flow channel is much narrower than the axial ones, which allows the fuel-air mixture to get in contact with the Pt on Al_2O_3 catalyst coated onto the pillar surface much more readily and thereby reduces the requirements of additional preheating of the on-chip microreactor and the initial fuel-air supplied. This is evident through a lower light-off temperature and starting flow rate for the diagonal flow configuration. It is to be noted that for the set of experiments conducted on four different designs, the recorded temperature trace with time for different flow rates suggests that the on-chip microreactor with squared pillared arrangement coupled with diagonal flow configuration provides the best performance of the catalytic combustion of methanol-air mixture in presence of Pt on Al_2O_3 catalyst based on lower light-off temperature, initial air flow rate, and achieved chip temperature.

As indicated in the existing literature (Resnik et al., 2012), the combustion of methanol-air mixture is characterized by a transition from heterogeneous catalytic combustion to a mixed heterogeneous-catalytic-and-homogeneous-gas-phase combustion. We also found a similar transition for our microreactors studied in this

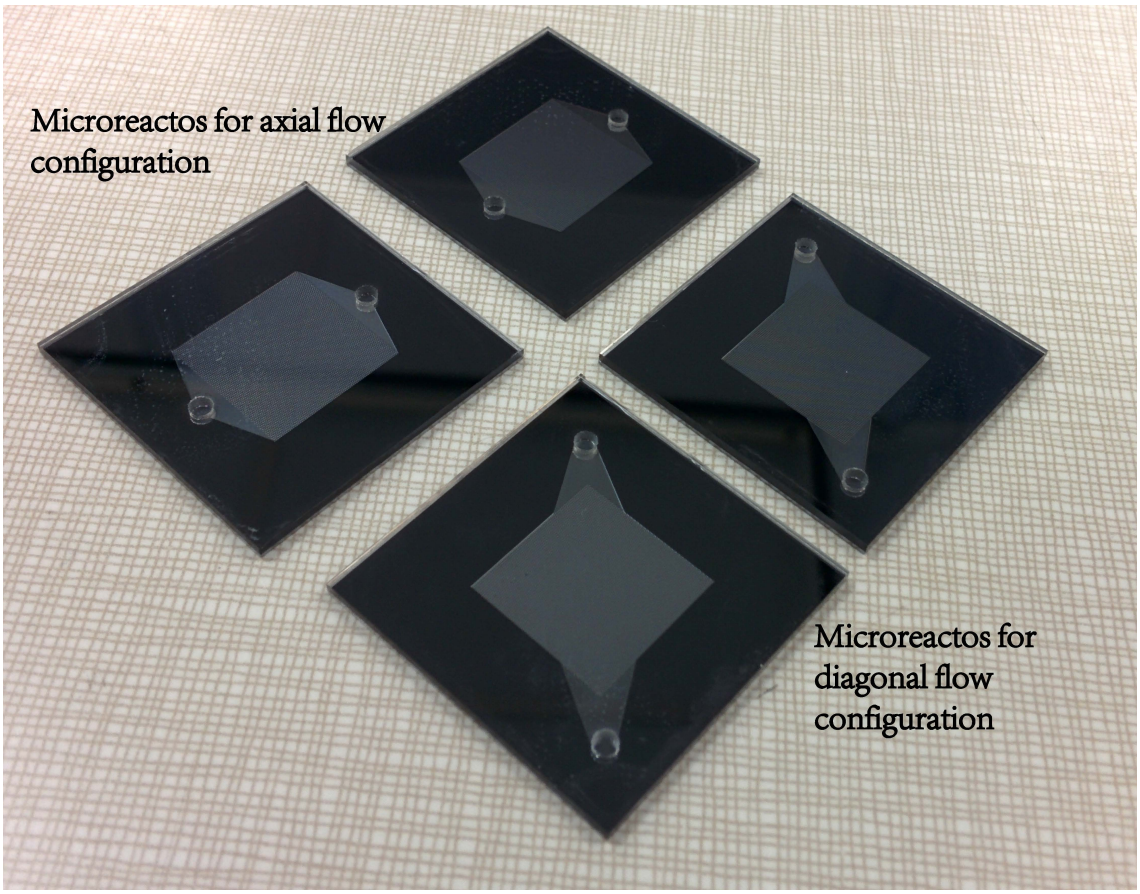

Figure 3.7: The microreactors with the diagonal flow configuration possess a inlet flow geometry much narrower than the axial ones.

work, which is illustrated in details in Figure 3.8, as a representative case for a microreactor with staggered pillar arrangement and diagonal flow configuration. For the sake of clarity, we have shown only a few experimental data points but the exponential fit to the data which have been obtained for at least 400 data points of each air flow rate. As shown in Figure 3.8, for Stages I, II, and III corresponding to air flow rate of 122.66 sccm, 164.33 sccm, and 207.39 sccm, respectively, we observed that for each such stage, the chip temperature would achieve a steady state value, which is indicated by means of a horizontal dashed line (exponential fit to the data) in the plot. However, when we changed the air flow rate at the end of Stage III from 207.39 sccm to 273.80 sccm, we observe a significant jump in the chip temperature ($\sim$12.5 $^{\circ}$C) as compared with the earlier stages ($\sim$ 4 $^{\circ}$C). This can be attributed to the transition phenomenon, as reported by Hu et al. (Hu et al., 2005).

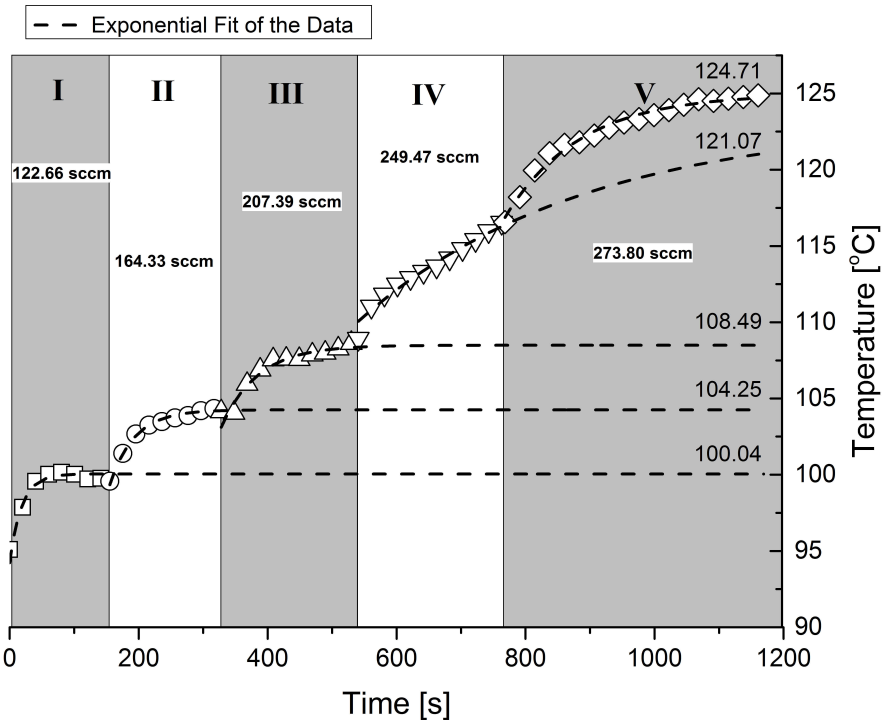

Figure 3.8: Measured temperature as a function of time for reactor with staggered pillar arrangement and diagonal flow configuration. The dashed line is for the piecewise exponential fit of the data. R^2 values for each flow rate from Stage I to Stage V are 0.96257, 0.98754, 0.95343, 0.97861, and 0.97974, respectively.

Chapter 4

Integration with Commercial Thermoelectric Module for Direct Thermal-to-Electric Conversion

4.1 On-chip Power Generation Introduction[1]

In the past decade, along with an increasing number of power-hungry hand-held electronic devices entering people's daily life, such as communicating, computing and entertainment equipments, there is a huge demand of portable power generating and supplying systems with higher energy density and longer-operational life. However, the research development of rechargeable batteries, which are the main choice of power source nowadays, is quite slow compared with the rapid evolution of electronic devices, making the "portable power gap" even larger. Furthermore, environmental issues caused by heavy metals and toxic chemicals contained in discarded batteries restrict its future progress. Therefore, the researchers had to turn their attention to other energy conversion methods.

Hydrocarbon fuels, compared with conventional batteries, have several orders of magnitude higher energy density. For example, the energy density of methanol (19.7 MJ/kg) is nearly 27 times higher than Li-ion batteries (0.72 MJ/kg). Also, hy-

[1]A version of this section has been published in *ASME 2013 International Mechanical Engineering Congress and Exposition*, November, 2014, Sheng Tian, Thomas Thundat, Subir Bhattacharjee, Kenneth C. Cadien, and Sushanta K. Mitra, (pp. V07BT08A005-V07BT08A005), American Society of Mechanical Engineers.

drocarbon fuels possess the advantages of availability and portability. Massive research efforts have been made to design and create portable power generators based on hydrocarbon fuels, which are considered as appropriate alternatives for conventional batteries. Taking methanol for instance, there are already several existing types of fuel cell systems that make use of the high energy density of methanol, such as reformed hydrogen fuel cells (Holladay et al., 2004; Kreuer, 2001) and direct fuel cell (Motokawa et al., 2004; Torres et al., 2008). However, they still suffer from poor performance of separation membrane, methanol cross-over and catalyst poisoning, especially CO.

Direct thermal-to-electric energy conversion using a thermoelectric platform is an promising method for power generation due to its higher energy density, containing no moving parts, quiet and environmentally friendly features compared with other conventional energy conversion methods such as the internal combustion engine or a chemical battery. (Goldsmid, 1986) Because of Seebeck effect, if a combustor as the heat source is placed on the hot side of a thermoelectric device, electricity can be produced from the temperature difference between the hot and cool regions conjuncted by thermoelectrical material. A detailed review about thermoelectric device and its power generation principle can be found in (DiSalvo, 1999).

It is long known that Platinum (Pt) particles can facilitate combustion of methanol. Hu Z. et al. (Hu et al., 2005) achieved stable self-ignition and self-supporting combustion of methanol at room temperature by introducing methanol/air vapor into a glass tube reactor filled with quartz glass wool deposited with Pt nanoparticles (NPs). Gas chromatographic (GC) analysis of the combustion gas products confirms the complete reaction of methanol, which is shown in Equation (4.1):

$$CH_3OH(l) + \frac{3}{2}O_2 \rightarrow CO_2 + 2H_2O,\ \Delta H^\circ = -639kJ/mol \tag{4.1}$$

Karim A. M. et al. (Karim et al., 2008) studied the catalytic self-ignition of methanol over Pt nanoparticles dispersed on an anodized alumina wafer. By adjust-

ing the flow rate of air and mole fraction of methanol introduced into a microburner, the highest temperature of the burner wall could be increased to more than 600°C. They also proposed that high flow rates and relatively lower fuel content would significantly reduce the start-up time for reaching the steady state of the system.

In this chapter, a design of entire operating system for on-chip microreactors is presented in details. We have already fabricated a batch of microfluidic-based reactors with integrated micropillars with standard optical lithography and deep reactive-ion etching (DRIE) technique. Using these microfluidics-based reactors, on-chip catalytic combustion of methanol-air mixture was achieved. By using such reactors as the heat source for commercial thermoelectric modules, on-chip power generation is expected to be achieved.

4.2 On-chip Power Generation Apparatus Configuration

4.2.1 Electric System Design

As the experimental results show in Chapter 3, a preheating process should be provided to start and sustain the catalytic combustion of methanol-air mixture over Pt on Al_2O_3 within the microreactors we fabricated. In such case, one usually uses "hydrogen-assisted" catalytic combustion method (Deutschmann et al., 2000; Norton and Vlachos, 2005), in which, initial flow of fuel-air-H_2 is introduced. As the combustion of fuel-air mixture starts with the assistance of H_2, the H_2 flow is reduced gradually and the fuel flow is increased. Eventually, the catalytic combustion of fuel-air mixture is sustained. However, in such cases, the experimental set-up will be more complicated, which requires an additional cylinder for H_2 gas and another delivery tubing would be needed. Also H_2 is much more hazardous, as it is extremely reactive with oxygen and needs very low ignition energy.

As we are using thermoelectric module in our system, according to Peltier effect, if we provide a current flow through the module, heat will be generated at

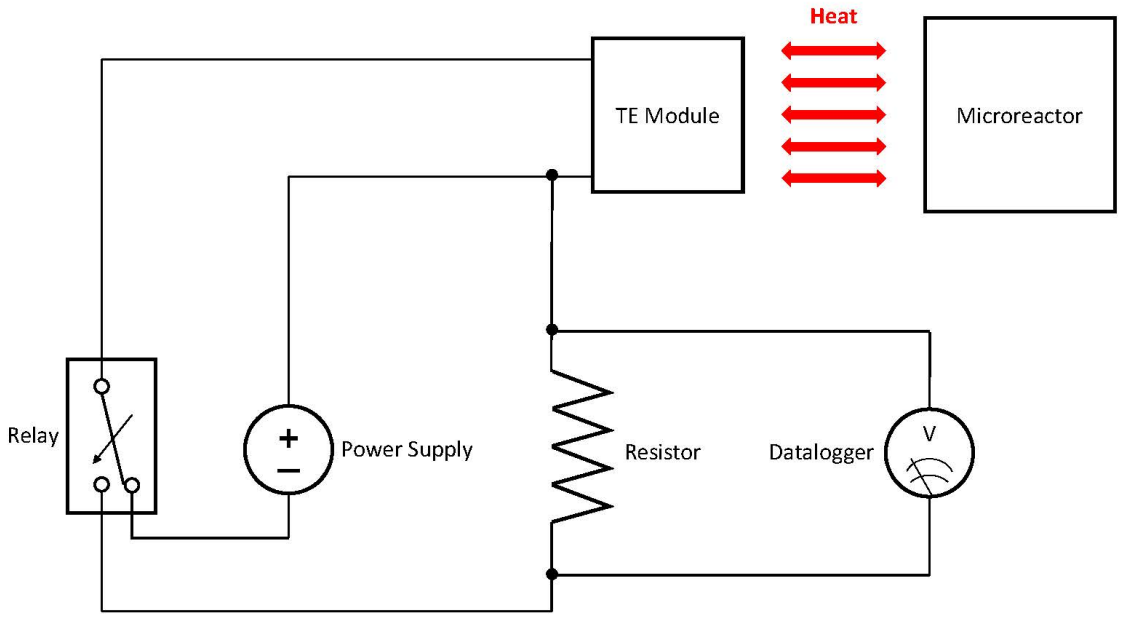

Figure 4.1: Electric system design to provide power for pre-heating and then achieve voltage measurement.

the hot side, which can be utilized to pre-heat the catalytic microreactor. Meanwhile, after the catalytic combustion of methanol-air mixture is stable, the current supplying can be shut down, then according to the Seebeck effect, the temperature difference maitained between the hot and cold side of the thermoelectric module will start creating voltage. Therefore, as shown in Figure 4.1, we designed a electric circuit installed in a box which satisfied all the requirements as described above.

The relay was used to switch the system from "Power Supplying" mode to "Power Generation" mode. During "Power Supplying" mode, the power supply will provide the current needed for the thermoelectric module to pre-heat the catalytic reactor. After the switch, during "Power Generation" mode, the heat generated by the catalytic combustion will be converted to electric power by the thermoelectrc module which maintain a voltage across the resistor. The datalogger connected will record the voltage trace with time under various conditions.

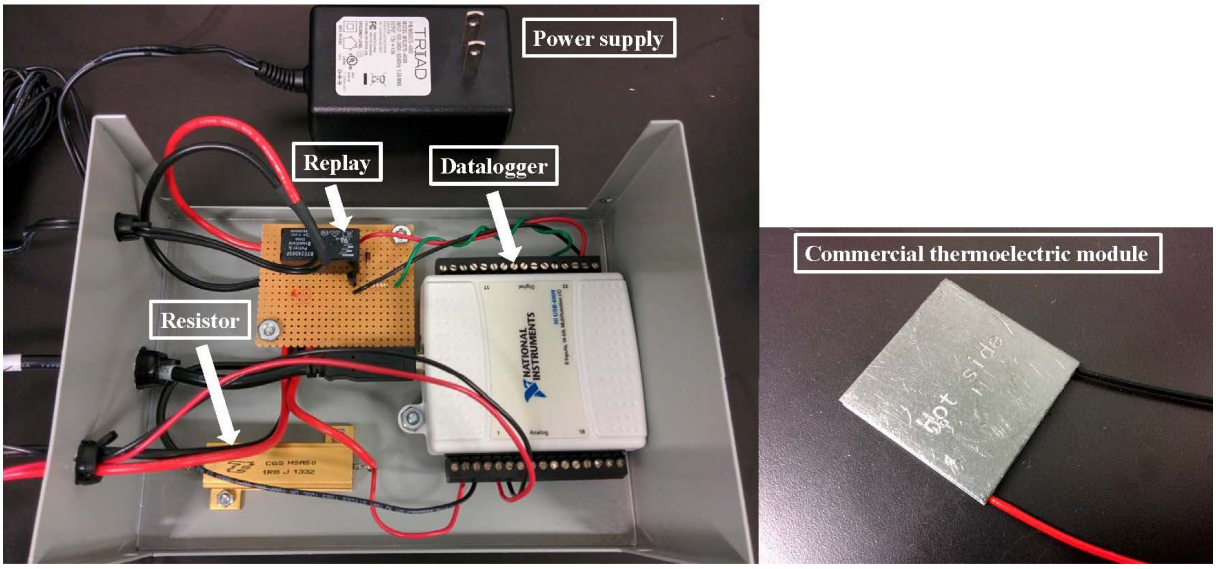

Figure 4.2: Experimental apparatus with "Power Supplying" and "Power Generation" modes assembled in the box.

4.2.2 Apparatus and Control

The electric apparatus assembled and installed in the box with the commercial thermoelectric module (from Custom Thermoelectric, Inc., USA) is shown in Figure 4.2. The control system which can switch the relay from "Power Supplying" mode to "Power Generation" mode was programed in LabView (National Instruments Corporation, USA). The User Interface of the control system as shown in Figure 4.3 also integrates a monitoring unit which can record the temperature of the thermoelectric module and shut down the system anytime when the temperature reaches beyond the safety limited (200°C, as per the reference temperature provided by the manufacturer).

The load resistance used in the electric circuit will be set as the same as thermoelectric module's average internal resistance. The power P of the module can be expressed as Equation (4.2):

$$P = R_L \left(\frac{U}{R_L + R_I} \right)^2 \tag{4.2}$$

Where, U is the voltage of the module, R_L and R_I are for the load resistance and

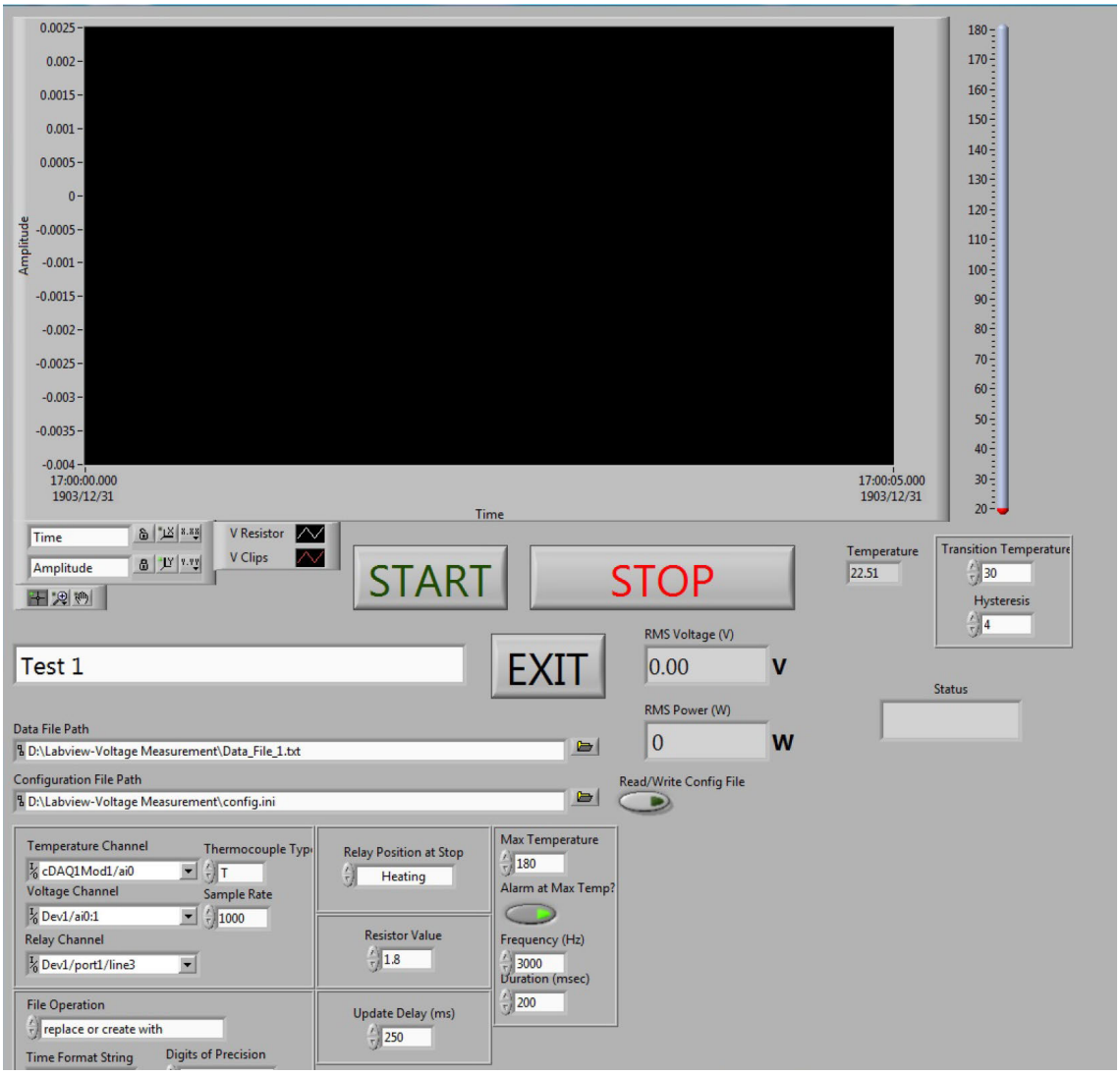

Figure 4.3: User Interface of the control system built in LabView.

thermoelectric module's internal resistance respectively. When R_L matches R_I, we can get the maximum power supplied from this on-chip power generation apparatus.

Thus, the electric system together with the thermoelectric module can be integrated into entire experimental set-up for the characterization of catalytic combustion to achieve power generation on-chip in a direct thermal-to-electric energy conversion platform, which is depicted in Figure 4.4. Such platform includes a chip-holder, whose completely assembled view is shown in Figure 4.4(b) and exploded view consisting of plastic cover, on-chip microreactor, commercial thermoelectric module, stainless steel base and heat sink is shown in Figure 4.4(c). The thermoelectric module is connected with the electric apparatus box consisting of relay, power supply, resistor and datalogger as shown in Figure 4.4(d), which can be set as the "Power Supplying" mode or "Power Generation" mode.

During the "Power Supplying" mode, the air coming out of the cylinder would flow through the wash bottle after regulated by the flowmeter, carrying methanol vapor into the microreactor supported in the chip-holder. The internal surface of on-chip microreactor would have been coated with Pt on Al_2O_3 catalyst as illustrated for detailed in Chapter 2. Consequently, with the help of pre-heating provided by the thermoelectric module powered by the electric apparatus, on-chip catalytic combustion of methanol-air mixture can be sustained. Then, one can use the control system to switch the relay from "Power Supplying" mode to "Power Generation" mode. After the entire system reach a stable state, the heat generated from the on-chip catalytic combustion would maintain a temperature difference between the hot and cold sides bridged by thermoelectric module. Therefore, the thermal energy from the combustion can be converted to electric energy because of the Seebeck effect. The data of voltage trace with time across the resistor in the electric circuit can be recorded continuously by the datalogger.

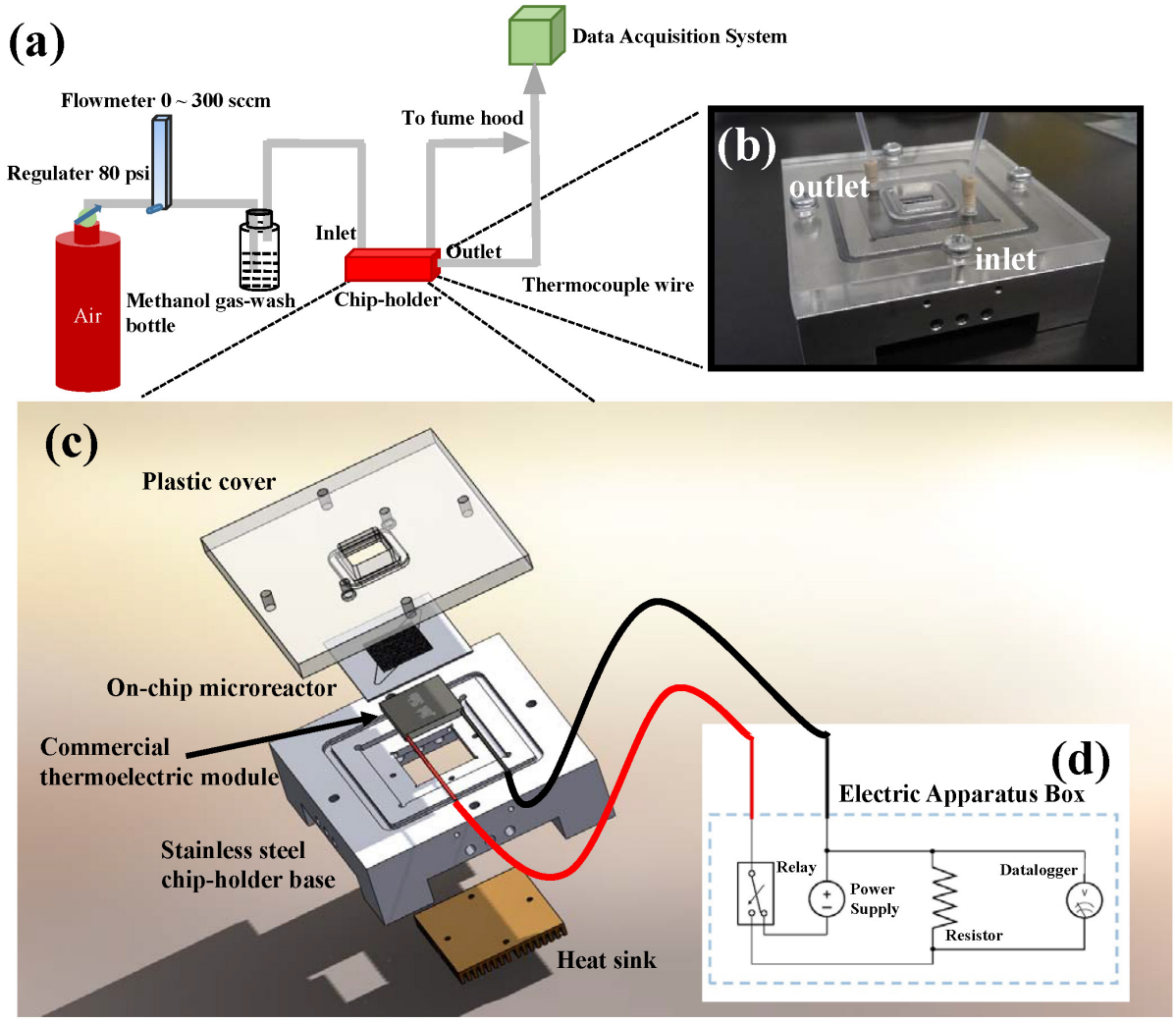

Figure 4.4: (a) Entire experimental set-up of direct thermal-to-electric energy conversion platform utilizing the catalytic combustion of methanol-air mixture within microfabricated on-chip microreactor. (b) Assembly of the chip-holder, on-chip microreactor and inlet/outlet ports. (c) Exploded view of the chip-holder (plastic cover, stainless steel chip-holder base) on-chip microreactor (for squared pillar arrangement and diagonal flow configuration), commercial thermoelectric module and heat sink. (d) Electric apparatus box consisting of relay, power supply, resistor and datalogger

Chapter 5

Conclusions and Future Prospects

5.1 Concluding Remarks

In this work, for the first time, we have successfully demonstrated catalytic combustion of the methanol-air mixture inside on-chip microreactors with integrated pillars. We have microfabricated four different microreactors on silicon substrate which have squared and staggered arrangements of pillars along with axial and diagonal flow configurations with standard optical lithography, deep reactive-ion etching (DRIE) and other fabrication techniques. With anodic borofloat glass cover to silicon substrate bonding and diamond touch dicing, closed microreactors ready for proper fuel-air mixture delivery were obtained.

We have tried the surface-selective infiltration method for catalyst deposition before bonding process which is based on water-ethanol-Pt-NPs suspension drop deposition to silicon substrate. However, SEM images showed poor uniformity and bad distribution of catalyst particles, as this method suffered from coffee ring effect. Therefore, wash-coating technique was explored and extremely small amount ($\sim$1.1 mg) of Pt on Al_2O_3 as catalyst was successfully deposited onto the reactor surfaces. The slurry was prepared by mixing Pt/Al_2O_3, deionized water and colloidal nano-sized alumina binders gel.

The chip-holder composed of plastic covers for different flow configurations and stainless steel base for microreactor and integrated thermoelectric module were de-

signed and manufactured. The entire experimental set-up consisting of compressed air cylinder with regulator, flowmeter, methanol gas-wash bottle chip-holder assembly, thermocouple wires as well as data acquisition and visualization system were built. With the help of proper tubings, fittings and connections, such experimental system is leakage-proof and capable of achieving on-chip catalytic combustion, data collection and experiment monitoring simultaneously.

Careful measurement of the microreactor temperature trace with time for different flow rates reveals that the squared pillar arrangement with diagonal flow configuration provides the best performance in terms of lower light-off temperature, initial air flow requirements and achieved average chip temperature. Furthermore, for axial flow configuration, changing the pillar arrangement from squared to staggered increases the mixing of methanol-air inside the chip and promotes higher average temperature. On the other hand, for diagonal flow configuration, squared arrangement always provides the higher average chip temperature. Regarding the light-off temperature and starting air flow rate, conditions microreactors with diagonal flow configuration needed to sustain autonomous catalytic combustion were much easier as compared to the ones with axial flow configuration. (95 °C and 122.66 sccm for diagonal flow configuration, 111 °C and 207.39 sccm for axial ones.)

We have also demonstrated that the combustion process in these on-chip microreactors is characterized by the well-known transition from heterogeneous catalytic combustion to a mixed heterogeneous-catalytic-and-homogeneous-gas-phase combustion. For a microreactor with staggered pillar arrangement and diagonal flow configuration, as we increased the air flow rate from 207.39 sccm to 273.80 sccm, a significant increment in temperature ($\sim$12.5 °C) was found. As the chip temperature increment is depended on reaction rate, such transition indicated that a huge jump of reaction rate took place at the point.

Such sustained catalytic combustion inside an on-chip microreactor can be utilized as a future heat source for an integrated direct thermal-to-electric energy plat-

form where the microreactor can be packaged with a thermoelectric module to increase the overall conversion efficiency of the system. An entire apparatus composed of power supplying for pre-heating the on-chip microreactor, power generation (integrated resistor) and measurement system (datalogger) were also designed for future work.

5.2 Future Work

Future work and improvement on this Nano-Catalytic Energy Cell project we are working on shall be focusing on the following aspects:

- Optimized geometric configuration of the microreactor for lower light-off temperature and starting air flow rate should be explored.
- Better catalyst with higher dispersion of active sites and lower cost should be explored. Not only Pt, other nanoparticles, such as Pd, with different supports shall be tested. If necessary, we need to fabricate catalyst from precursors by ourselves.
- Other catalytic deposition method, for example, atomic layer deposition can be tried to form nanoparticles on silicon substrate directly.
- Combining optimized geometric configuration of the microreactor and better performing catalyst, on-chip catalytic combustion of fuel-air mixture is expected to be sustained from room temperature. The pre-heating process will not be needed.
- Better thermoelectric module with higher a figure of merit, ZT, which depends on electrical conductivity, the thermal conductivity and the Seebeck coefficient.
- A prototype of direct thermal-to-electric energy platform utilizing optimized on-chip microreactor and better thermoelectric material shall be built to achieve on-chip power generation.

- Further miniaturizing the microreactor. Shrinking the size of fuel storage and supply system.
- The ultimate goal of this project is to put everything, the fuel delivery, on-chip catalytic combustion, thermal-to-electric conversion apparatuses in one box to make one portable power source as the final product.

References

Applegate, J. R., McNally, D., Pearlman, H., and Bakrania, S. D. (2013). Platinum-nanoparticle-catalyzed combustion of a methanol–air mixture. *Energy & Fuels*, 27(7):4014–4020.

Applegate, J. R., Pearlman, H., and Bakrania, S. D. (2012). Catalysis of methanol-air mixture using platinum nanoparticles for microscale combustion. *Journal of Nanomaterials*, 2012:9.

Arico, A., Srinivasan, S., and Antonucci, V. (2001). Dmfcs: from fundamental aspects to technology development. *Fuel cells*, 1(2):133–161.

Beebe, D. J., Mensing, G. A., and Walker, G. M. (2002). Physics and applications of microfluidics in biology. *Annual review of biomedical engineering*, 4(1):261–286.

Chen, H., Bednarova, L., Besser, R., and Lee, W. (2005). Surface-selective infiltration of thin-film catalyst into microchannel reactors. *Applied Catalysis A: General*, 286(2):186–195.

Deegan, R. D., Bakajin, O., Dupont, T. F., Huber, G., Nagel, S. R., and Witten, T. A. (1997). Capillary flow as the cause of ring stains from dried liquid drops. *Nature*, 389(6653):827–829.

Deutschmann, O., Maier, L., Riedel, U., Stroemman, A., and Dibble, R. (2000). Hydrogen assisted catalytic combustion of methane on platinum. *Catalysis Today*, 59(1):141–150.

DiSalvo, F. J. (1999). Thermoelectric cooling and power generation. *Science*, 285(5428):703–706.

Dyer, C. K. (2002). Fuel cells for portable applications. *Journal of Power Sources*, 106(1):31–34.

Faghri, A. and Guo, Z. (2005). Challenges and opportunities of thermal management issues related to fuel cell technology and modeling. *International Journal of Heat and Mass Transfer*, 48(19):3891–3920.

Federici, J. A., Norton, D. G., Brüggemann, T., Voit, K., Wetzel, E., and Vlachos, D. (2006). Catalytic microcombustors with integrated thermoelectric elements for portable power production. *Journal of Power Sources*, 161(2):1469–1478.

Firth, J. (1971). Catalytic oxidation of methanol over platinum. *Transactions of the Faraday Society*, 67:212–215.

Goldsmid, H. J. (1986). *Electronic refrigeration*, volume 76. Pion London.

Goodenough, J. B. and Kim, Y. (2009). Challenges for rechargeable li batteries. *Chemistry of Materials*, 22(3):587–603.

Gottesfeld, S. and Pafford, J. (1988). A new approach to the problem of carbon monoxide poisoning in fuel cells operating at low temperatures. *Journal of the Electrochemical Society*, 135(10):2651–2652.

Gunda, N. S. K., Joseph, J., Tamayol, A., Akbari, M., and Mitra, S. K. (2013a). Measurement of pressure drop and flow resistance in microchannels with integrated micropillars. *Microfluidics and nanofluidics*, 14(3-4):711–721.

Gunda, N. S. K., Naicker, S., Ghoraishi, M. S., Bhattacharjee, S., Thundat, T. G., and Mitra, S. K. (2013b). Microspot with integrated wells (msiw) for the detection of e. coli. In *ASME 2013 11th International Conference on Nanochannels, Microchannels, and Minichannels*, pages V001T10A001–V001T10A001. American Society of Mechanical Engineers.

Gunda, N. S. K., Singh, M., Purwar, Y., Shah, S. L., Kaur, K., and Mitra, S. K. (2013c). Micro-spot with integrated pillars (msip) for detection of dengue virus ns1. *Biomedical microdevices*, 15(6):959–971.

Gurau, B. and Smotkin, E. S. (2002). Methanol crossover in direct methanol fuel cells: a link between power and energy density. *Journal of Power Sources*, 112(2):339–352.

Han, K.-H. and Frazier, A. B. (2006). Paramagnetic capture mode magnetophoretic microseparator for high efficiency blood cell separations. *Lab on a Chip*, 6(2):265–273.

Hessel, V., Löwe, H., and Schönfeld, F. (2005). Micromixersa review on passive and active mixing principles. *Chemical Engineering Science*, 60(8):2479–2501.

Hibino, T., Hashimoto, A., Inoue, T., Tokuno, J.-i., Yoshida, S.-i., and Sano, M. (2000). A low-operating-temperature solid oxide fuel cell in hydrocarbon-air mixtures. *Science*, 288(5473):2031–2033.

Holladay, J. D., Wainright, J., Jones, E. O., and Gano, S. (2004). Power generation using a mesoscale fuel cell integrated with a microscale fuel processor. *Journal of power sources*, 130(1):111–118.

Hu, Z. (2007). Nanoscale energy conversion and its applications. In *2007 First International Conference on Integration and Commercialization of Micro and Nanosystems*, pages 909–915. American Society of Mechanical Engineers.

Hu, Z., Boiadjiev, V., and Thundat, T. (2005). Nanocatalytic spontaneous ignition and self-supporting room-temperature combustion. *Energy & fuels*, 19(3):855–858.

Hucknall, D. J. (1985). Chemistry of hydrocarbon combustion.

Jähnisch, K., Hessel, V., Löwe, H., and Baerns, M. (2004). Chemistry in microstructured reactors. *Angewandte Chemie International Edition*, 43(4):406–446.

Jensen, K. F. (2001). Microreaction engineeringis small better? *Chemical Engineering Science*, 56(2):293–303.

Karim, A., Federici, J., and Vlachos, D. (2008). Portable power production from methanol in an integrated thermoeletric/microreactor system. *Journal of Power Sources*, 179(1):113–120.

Kreuer, K. (2001). On the development of proton conducting polymer membranes for hydrogen and methanol fuel cells. *Journal of membrane science*, 185(1):29–39.

Ledjeff, K. and Nolte, R. (1999). Polymer electrolyte membrane fuel cell. US Patent 5,863,672.

Low, L.-M., Seetharaman, S., He, K.-Q., and Madou, M. J. (2000). Microactuators toward microvalves for responsive controlled drug delivery. *Sensors and Actuators B: Chemical*, 67(1):149–160.

Ma, Y., Ricciuti, C., Miller, T., Kadlowec, J., and Pearlman, H. (2008). Enhanced catalytic combustion using sub-micrometer and nano-size platinum particles. *Energy & Fuels*, 22(6):3695–3700.

Marton, C. H., Haldeman, G. S., and Jensen, K. F. (2011). Portable thermoelectric power generator based on a microfabricated silicon combustor with low resistance to flow. *Industrial & Engineering Chemistry Research*, 50(14):8468–8475.

Mason, B. P., Price, K. E., Steinbacher, J. L., Bogdan, A. R., and McQuade, D. T. (2007). Greener approaches to organic synthesis using microreactor technology. *Chemical reviews*, 107(6):2300–2318.

Mehta, V. and Cooper, J. S. (2003). Review and analysis of pem fuel cell design and manufacturing. *Journal of Power Sources*, 114(1):32–53.

Meille, V. (2006). Review on methods to deposit catalysts on structured surfaces. *Applied Catalysis A: General*, 315:1–17.

Men, Y., Fu, Y., Chen, Z., Sims, P. A., Greenleaf, W. J., and Huang, Y. (2012). Digital polymerase chain reaction in an array of femtoliter polydimethylsiloxane microreactors. *Analytical chemistry*, 84(10):4262–4266.

Motokawa, S., Mohamedi, M., Momma, T., Shoji, S., and Osaka, T. (2004). Mems-based design and fabrication of a new concept micro direct methanol fuel cell (μ-dmfc). *Electrochemistry Communications*, 6(6):562–565.

Murray, E. P., Tsai, T., and Barnett, S. (1999). A direct-methane fuel cell with a ceria-based anode. *Nature*, 400(6745):649–651.

Norton, D., Wetzel, E., and Vlachos, D. (2006). Thermal management in catalytic microreactors. *Industrial & engineering chemistry research*, 45(1):76–84.

Norton, D. G. and Vlachos, D. G. (2005). Hydrogen assisted self-ignition of propane/air mixtures in catalytic microburners. *Proceedings of the Combustion Institute*, 30(2):2473–2480.

Ormerod, R. M. (2003). Solid oxide fuel cells. *Chemical Society Reviews*, 32(1):17–28.

Park, S., Vohs, J. M., and Gorte, R. J. (2000). Direct oxidation of hydrocarbons in a solid-oxide fuel cell. *Nature*, 404(6775):265–267.

Pavlov, B. and Qiao, L. (2012). Catalytic oxidation of methanol on platinum nanoparticles. In *Spring Technical Meeting, the Central States Section of the Combustion Institute*, pages 22–24.

Resnik, D., Hočevar, S., Batista, J., Vrtačnik, D., Možek, M., and Amon, S. (2012). Si based methanol catalytic micro combustor for integrated steam reformer applications. *Sensors and Actuators A: Physical*, 180:127–136.

Rostrup-Nielsen, J. R. (2001). Conversion of hydrocarbons and alcohols for fuel cells. *Physical Chemistry Chemical Physics*, 3(3):283–288.

Schaevitz, S. B., Franz, A. J., Jensen, K. F., and Schmidt, M. A. (2001). A combustion-based mems thermoelectric power generator. In *The 11th International Conference on Solid-State Sensors and Actuators*, pages 30–33.

Smitha, B., Sridhar, S., and Khan, A. (2005). Solid polymer electrolyte membranes for fuel cell applicationsa review. *Journal of Membrane Science*, 259(1):10–26.

Srinivasan, R., Hsing, I., Berger, P. E., Jensen, K. F., Firebaugh, S. L., Schmidt, M. A., Harold, M. P., Lerou, J. J., Ryley, J. F., et al. (1997). Micromachined reactors for catalytic partial oxidation reactions. *AIChE Journal*, 43(11):3059–3069.

Steele, B. C. and Heinzel, A. (2001). Materials for fuel-cell technologies. *Nature*, 414(6861):345–352.

Tanaka, Y., Morishima, K., Shimizu, T., Kikuchi, A., Yamato, M., Okano, T., and Kitamori, T. (2006). An actuated pump on-chip powered by cultured cardiomyocytes. *Lab on a Chip*, 6(3):362–368.

Tarascon, J.-M. and Armand, M. (2001). Issues and challenges facing rechargeable lithium batteries. *Nature*, 414(6861):359–367.

Tian, S., Thundat, T., Bhattacharjee, S., Cadien, K. C., and Mitra, S. K. (2013). On-chip power generation: Microfluidic-based reactor for catalytic combustion of methanol. In *ASME 2013 International Mechanical Engineering Congress and Exposition*, pages V07BT08A005–V07BT08A005. American Society of Mechanical Engineers.

Torres, N., Santander, J., Esquivel, J., Sabaté, N., Figueras, E., Ivanov, P., Fonseca, L., Gràcia, I., and Cané, C. (2008). Performance optimization of a passive silicon-based micro-direct methanol fuel cell. *Sensors and Actuators B: Chemical*, 132(2):540–544.

Wagner, J. and Köhler, J. (2005). Continuous synthesis of gold nanoparticles in a microreactor. *Nano letters*, 5(4):685–691.

Wasmus, S. and Küver, A. (1999). Methanol oxidation and direct methanol fuel cells: a selective review. *Journal of Electroanalytical Chemistry*, 461(1):14–31.

Winter, M. and Brodd, R. J. (2004). What are batteries, fuel cells, and supercapacitors? *Chemical reviews*, 104(10):4245–4270.

Yadav, S., Sharma, P., Yamasani, P., Minaev, S., and Kumar, S. (2014). A prototype micro-thermoelectric power generator for micro-electromechanical systems. *Applied Physics Letters*, 104(12):123903.

Yoshida, K., Tanaka, S., Tomonari, S., Satoh, D., and Esashi, M. (2006). High-energy density miniature thermoelectric generator using catalytic combustion. *Microelectromechanical Systems, Journal of*, 15(1):195–203.

Yuan, W., Deng, J., Zhou, B., Zhang, Z.-c., and Tang, Y. (2014). Performance of a catalytic micro-combustor based on pt al2o3 ni for methanol fuel cell application. *Chemical Engineering Journal*, 251:51–57.

Appendix A

Appendix

A-1 Detailed Fabrication Techniques Used

In this section, we report the fabrication techniques used in details. All the microfabrication work was done in the University of Alberta Nanofabrication and Characterization Facility (nanoFab). The glass covers were water-jet cut with the help of technical staff member in machine shop, Department of Mechanical Engineering, University of Alberta. The same procedure was followed as described in Chapter 2.

A-1.1 Mask Design and Fabrication

A photo mask is a piece of chrome-coated glass with which we can transfer the pattern designed onto silicon wafer during optical lithography process. We designed our photo mask pattern with L-Edit software (Tanner EDA Inc., USA), which is shown in Figure A-1. Four different models with two different micropillar arrangements, viz., squared and staggered, and two different flow configurations, viz., axial (i.e., pillars are aligned with the flow direction) and diagonal (i.e., pillars are at 45° to the flow direction) were generated. Each model consists of microfluidic ports, inlet and outlet regions and an area of 15 mm $\times$ 15 mm with an array of 75 $\times$ 75 micropillars.

The final mask with the designed pattern on top was fabricated by etching the chrome layer from the glass substrate using a laser.

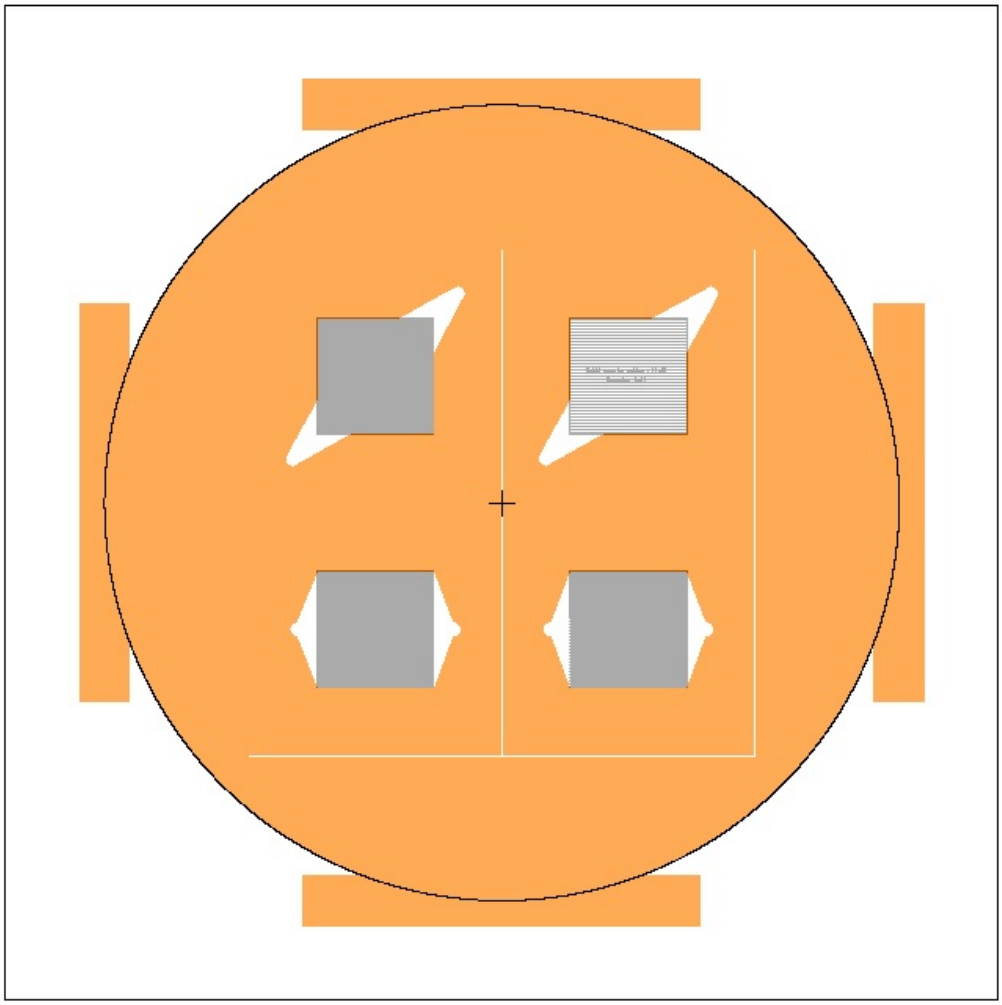

Figure A-1: Photo mask pattern designed with L-Edit.

A-1.2 Silicon Substrate

The 4-inch silicon substrates used in this work were purchased from nanoFab, University of Alberta. These wafers were thermally oxidized with $\sim$500 nm SiO_2 layer, which is intended as etching mask layer.

A-1.3 HDMS (hexamethyldisilazane) Deposition

The silicon substrates were firstly placed in YES HMDS Oven for one cycle to be coated with a layer of HDMS (hexamethyldisilazane), which promotes adhesion of photo resist to silicon dioxide layer. This process was done automatically.

A-1.4 Coating of Photoresist

The photoresist used in this work was positive photoresist (PPR) HPR 506 from Fuji-film Electronic Materials, Inc., USA. 5-10 mL HPR was poured onto the center of the wafer and spin the resist at the following parameters: (1) Spread: 500 RPM for 10 s; and (2) Spin: 4000 RPM for 40 s in Solitec Spinner (Solitec Wafer Processing, Inc., USA). Post bake was performed using Solitec vacuum hotplate at 115 °C for 90 s. After post baking, the wafers must be rehydrated for about 15 min, which is quite important for proper exposure and developing of the resist later.

A-1.5 Optical Lithography

The ABM Mask Aligners was used to transfer a pattern designed on photo mask to the HPR-coated silicon substrates by UV light. The exposure time used was 3.5 s.Appropriate chuck and mask frame should be chose and set for our 4-inch silicon wafers.

A-1.6 HPR Development

We used 354 developer to remove the non-UV-exposed HPR. The developing time is 25 s. It is to be noted that, the developing reslut should be inspected that whether the features of the pattern are kept and the un-wanted areas are removed. The substrates should be re-developed or even re-UV-exposed if necessary.

A-1.7 Etching Process

SiO_2 layer was etched using STS RIE system in 2 min 30 s, which was followed by etching of Si for $\sim$ 100 μ in 65 cycles using Bosch deep reactive-ion etching (DRIE) method with STS ICP-RIE system. As we observed, PPR was also etched during this process due to the selectivity of the etching systems. The residual PPR was cleaned by oxygen plasma process using Branson Barrel etcher before removing the SiO_2 layer underneath using STS RIE system again.

The chambers of STS RIE system and STS ICP-RIE system were both preconditioned before processing the silicon wafers. SiO_2 layer serves as etch mask to withstand the etching processes.

A-1.8 Glass Cover Design and Cutting

Borofloat glasses intended for covering the silicon substrates with integrated micropillars were purchased from nanoFab, University of Alberta. The inlet and outlet holes were drilled using abrasive water-jet cutter (2652 Jet Machining Center, USA) in machine shop, Department of Mechanical Engineering, University of Alberta.

The drawing for water-jet cutting is shown in Figure A-2, which was designed in Solidworks (SOLIDWORKS Corp., USA).

A-1.9 Piranha Cleaning

Piranha Cleaning was done prior to glass-silicon bonding process to make sure no particles or any other dust remained on both glass and silicon wafers. Piranha bath was prepared by slowly pouring the required amount of Sulphuric Acid into Hydrogen Peroxide (volume ratio: $H_2SO_4 : H_2O_2 = 3 : 1$) in a glass beaker.

It is to be noted that the mixing is an exothermic reaction, the temperature will be very high. Also, because both H_2SO_4 and H_2O_2 are strong oxidizer and corrosive

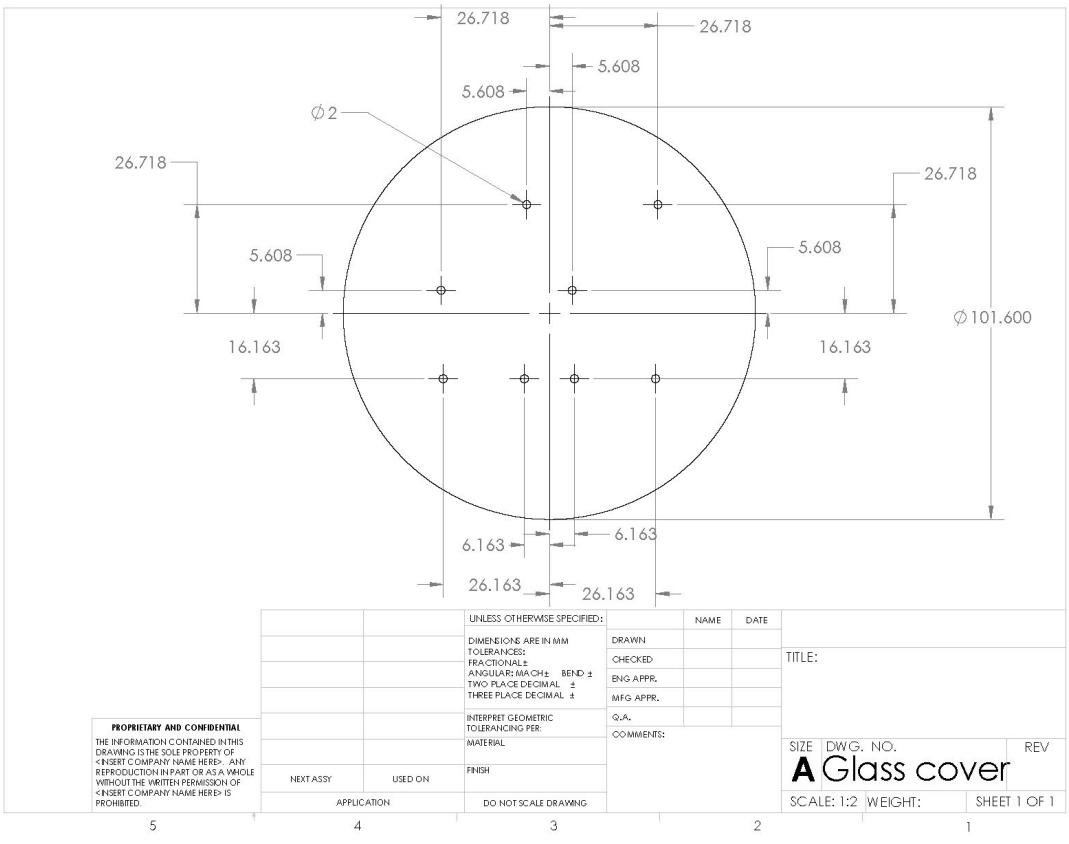

Figure A-2: Drawing for borofloat glass cover with inlet and outlet holes

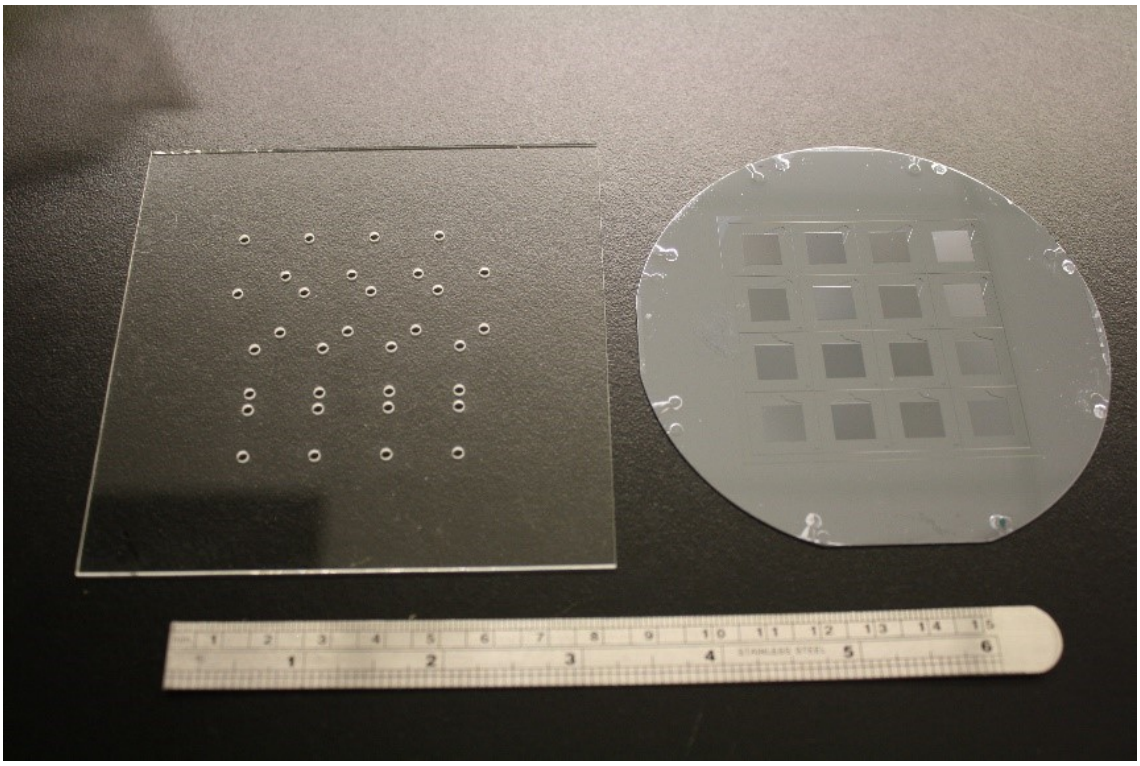

Figure A-3: A set of glass and Si substrate.

liquid, appropriate Acid Gear, for example, Chemical Apron, Chemical Resistant Gloves and Face Shield must be worn during the whole cleaning process.

All the silicon and glass substrates should be transferred into the Piranha bath using a Teflon carrier. The bath time was set as 15 m. Afterward, putting the substrates in dump rinser for 5 full cycles was done to remove all Piranha solution before drying them with Spin Rinse Dryer.

A set of glass cover drilled with inlet and outlet holes and Si substrate with integrated micropillars is shown in Figure A-3.

A-1.10 Glass to Silicon Bonding

An anodic bonding recipe applying high temperature and high pressure was used to the borofloat glass drilled with inlet and outlet holes to the micropillar integrated Si substrate in SUSS bonder (SÜSS MiroTec AG, Germany). The temperature was

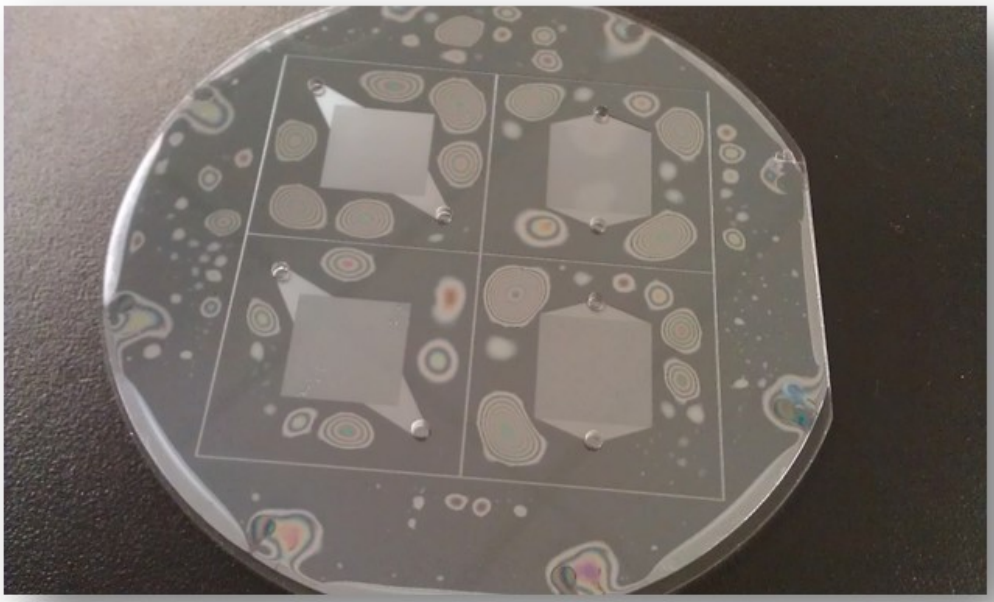

Figure A-4: Silicon substrate bonded with borofloat glass on top.

set as 350 °C.

An unsuccessful example of resulted borofloat glass covered Si wafer is shown in Figure A-4. Those Newton's rings structure indicated there were unfavorite particles existing in between. This shows even after Piranha cleaning, if the wafers were kept in clean room, they might be contaminated, which would affect the bonding result. Proper cleaning with Spin Rinse Dryer must be needed right before bonding.

A-1.11 Bonded Substrate Dicing

The bonded borofloat glass covered Si wafer was diced by dicing saw (Diamond Touch). Two layers of tape must be used while loading the substrate onto the cutting frame. The tapes will prevent the chance of cutting the chuck and breaking blade.

Table A.1: Geometrical Parameters of Different Reactors Designed

Notations	D (μm)	H (μm)	S (mm^2)	V (mm^3)	S/V (m^{-1})
90_SQ_AX	90	85	190.81	2.36	80.80
90_ST_AX	90	85	190.81	2.36	80.80
90_SQ_DI	90	85	190.81	2.36	80.80
90_ST_DI	90	85	190.81	2.36	80.80
70_SQ_AX	70	85	171.80	3.80	45.23
70_ST_DI	70	85	171.80	3.80	45.23
70_SQ_DI	70	85	171.80	3.80	45.23
70_ST_DI	70	85	171.80	3.80	45.23
50_SQ_DI	50	85	148.56	4.88	30.47
50_ST_DI	50	85	148.56	4.88	30.47
50_SQ_DI	50	85	148.56	4.88	30.47
50_ST_DI	50	85	148.56	4.88	30.47
30_SQ_DI	30	85	121.10	5.59	21.65
30_ST_DI	30	85	121.10	5.59	21.65
30_SQ_DI	30	85	121.10	5.59	21.65
30_ST_DI	30	85	121.10	5.59	21.65

A-2 Preliminary Fabrication Results[1]

During the preliminary fabrication test, we generated 16 models on silicon substrate all with an area of 8.4 mm $\times$ 8.4 mm with an array of 82 $\times$ 82 micropillars. These reactors were designed for different pillar diameters (90 μm, 70 μm, 50 μm, 30 μm), different pillar arrangement (square, staggered) and different flow directions (axially, diagonally). The parameters of the designed reactors on one silicon wafer is shown in Table A.1. Here, D is the diameter of the pillar, H is the height of the pillar or the etching depth, S is the internal surface area, V is the internal volume, S/V is the surface-area-to-volume-ratio. SQ and ST are for square and staggered pillar arrangements, respectively. AX is the notation for axially flow direction while DI is for diagonally flow direction.

Figure A-5 shows the scanning electron microscope (SEM) images of the fabri-

[1]A version of this section has been published in *ASME 2013 International Mechanical Engineering Congress and Exposition*, November, 2014, Sheng Tian, Thomas Thundat, Subir Bhattacharjee, Kenneth C. Cadien, and Sushanta K. Mitra, (pp. V07BT08A005-V07BT08A005), American Society of Mechanical Engineers.

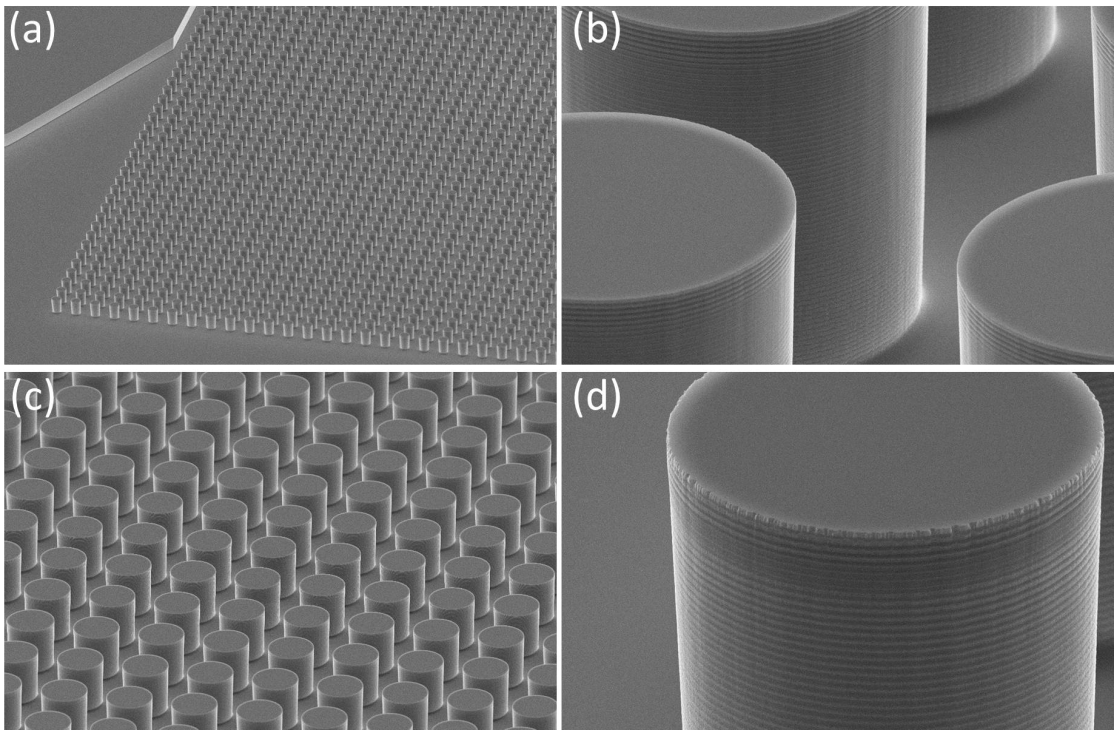

Figure A-5: SEM Images of Micropillars Fabricated On Silicon Wafer. (a) 50_SQ_DI (b) Magnified Image of 50_SQ_DI (c) 70_ST_DI (d) Magnified Image of 70_ST_AX

cated micropillars. It is observed that the undulating sidewall profiles on the surface of these micropillars were formed due to the Bosch DRIE process.

The schematic of fabricated on-chip microreactors with integrated micropillars is shown in Figure A-6.

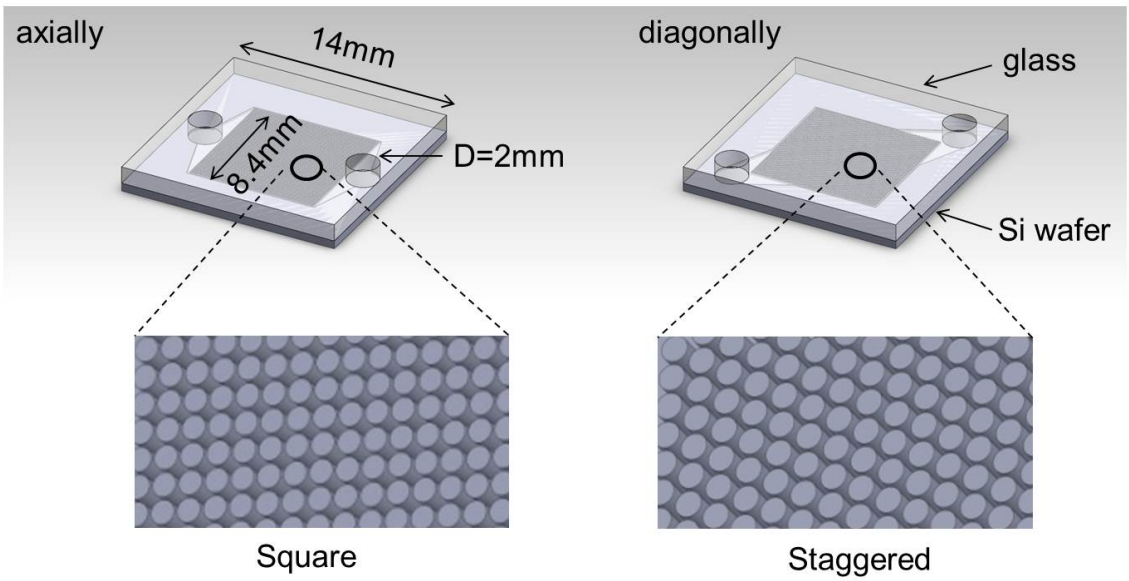

Figure A-6: Schematic of Fabricated On-chip Microeactors with Integrated Micropillars.

A-3 Chip-holder Design and Manufacture

As shown in chapter 3, Figure 3.1(b), the stainless steel part of the chip-holder (base) possesses two slots, one for on-chip microreactor, the other for commercial thermoelectric module. The reactor will get contact with the thermoelectric module tightly in the meanwhile providing heat if on-chip catalytic combustion of methanol-air mixture is sustained, so that on-chip power generation is expected to be achieved. Thermocouple wires can be placed on the hot or cool side of the thermoelectric module through the drilled holes to measure the temperature difference. Also there are two plastic covers for different flow configurations made from PDMS which are designed to make the system close and form appropriate fuel delivery with the help of inlet and outlet tubes as well as fittings.

All the parts of the chip-holder assembly were designed in Solidworks (SOLIDWORKS Corp., USA) and manufactured in machine shop, Department of Mechanical Engineering, University of Alberta.. The drawings of the plastic covers for axial and diagonal flow configurations as well as stainless steel base are show in Figure A-7, Figure A-8, and Figure A-9 respectively.

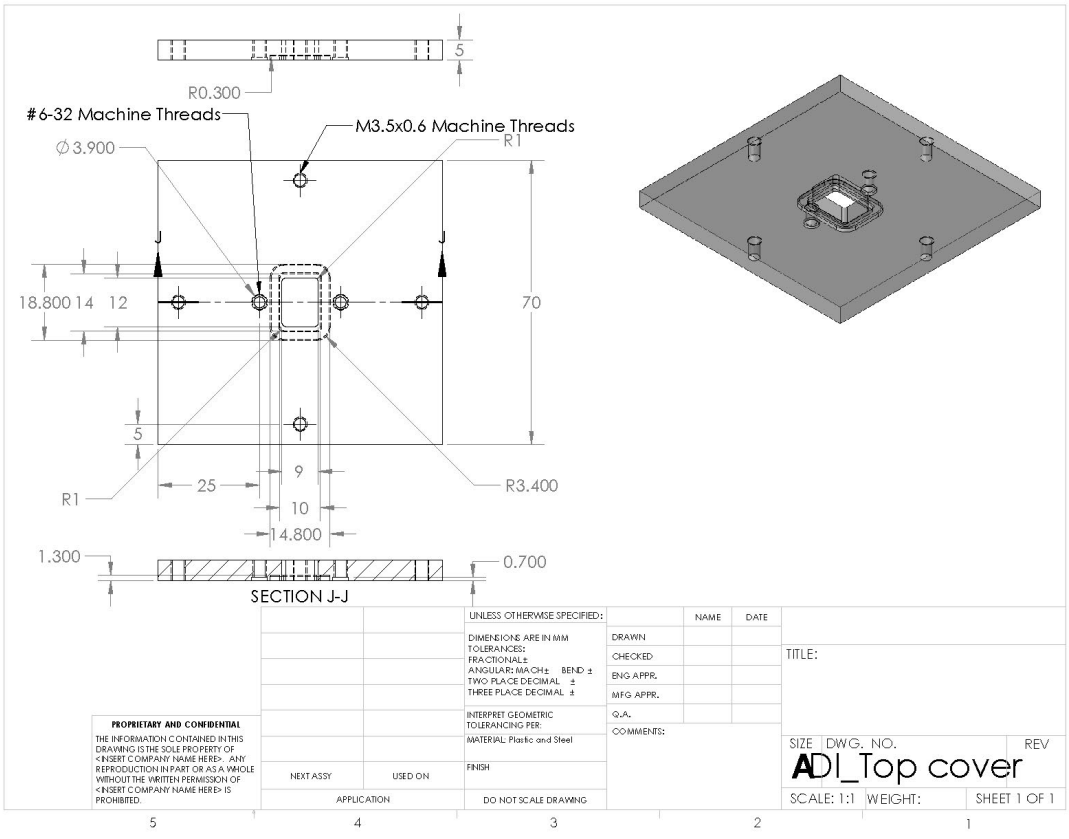

Figure A-7: Drawing of plastic cover with inlet and outlet ports for axial flow axial flow configuration.

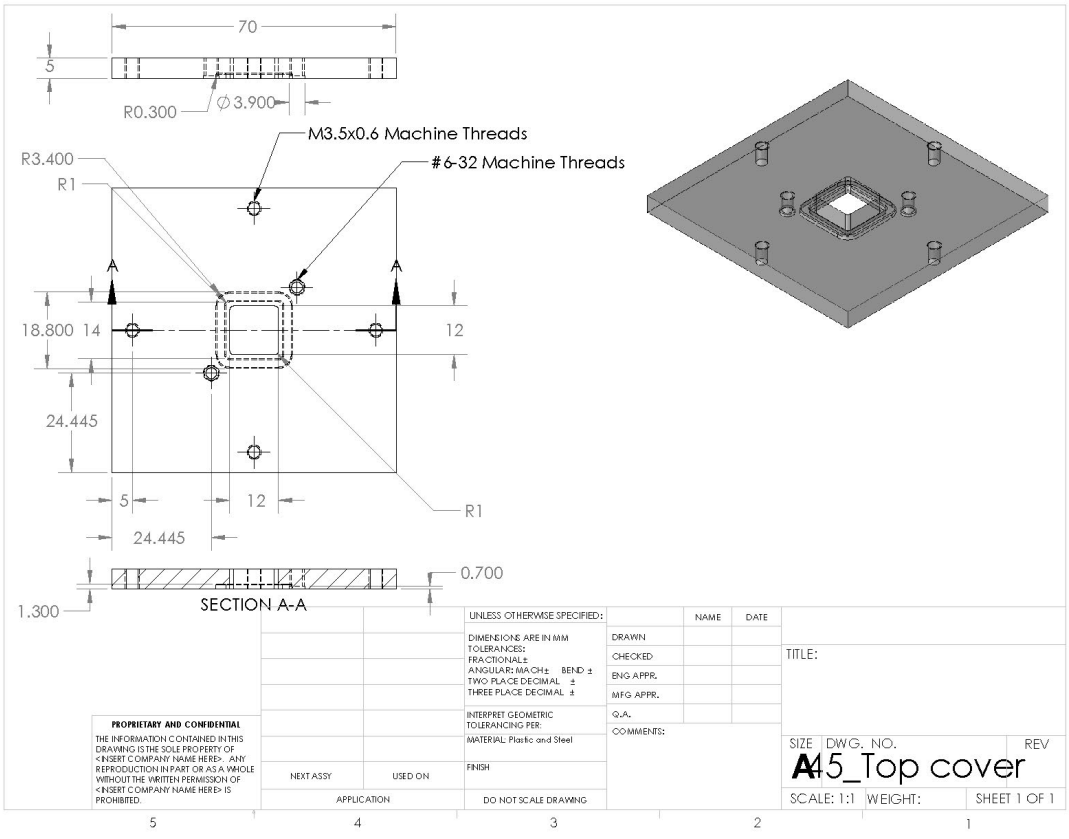

Figure A-8: Drawing of plastic cover with inlet and outlet ports for axial flow diagonal flow configuration.

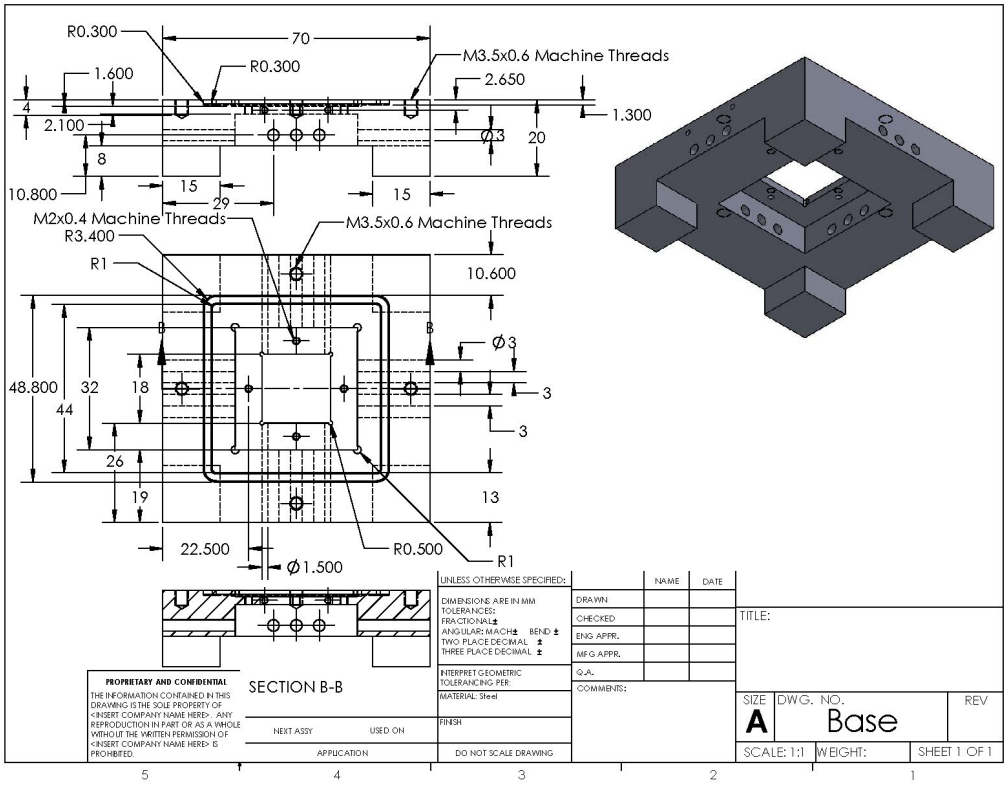

Figure A-9: Drawing of base for the chip-holder.

A-4 Raw Data Analysis

Temperature measurement of all four on-chip microreactors as a function of time is shown in Figure A-10. Here, AX and DI are for axial flow direction and diagonal flow direction, while SQ is the notation for square pillar arrangements and ST is for staggered pillar arrangement.

It clearly shows the difference of light-off temperature between reactors with axial flow direction and diagonal flow direction, as 95 °C for diagonal flow configuration, while 111 °C for axial ones. This phenomenon was discussed in chapter 3.

Figure A-11 shows the different stages corresponding to air flow rate of 122.66 sccm, 164.33 sccm, 207.39 sccm, 249.47 sccm, 278.80 sccm and 0 sccm respectively. In this process, we increased the air flow rate gradually and then shut down the valve of flowmeter at last.

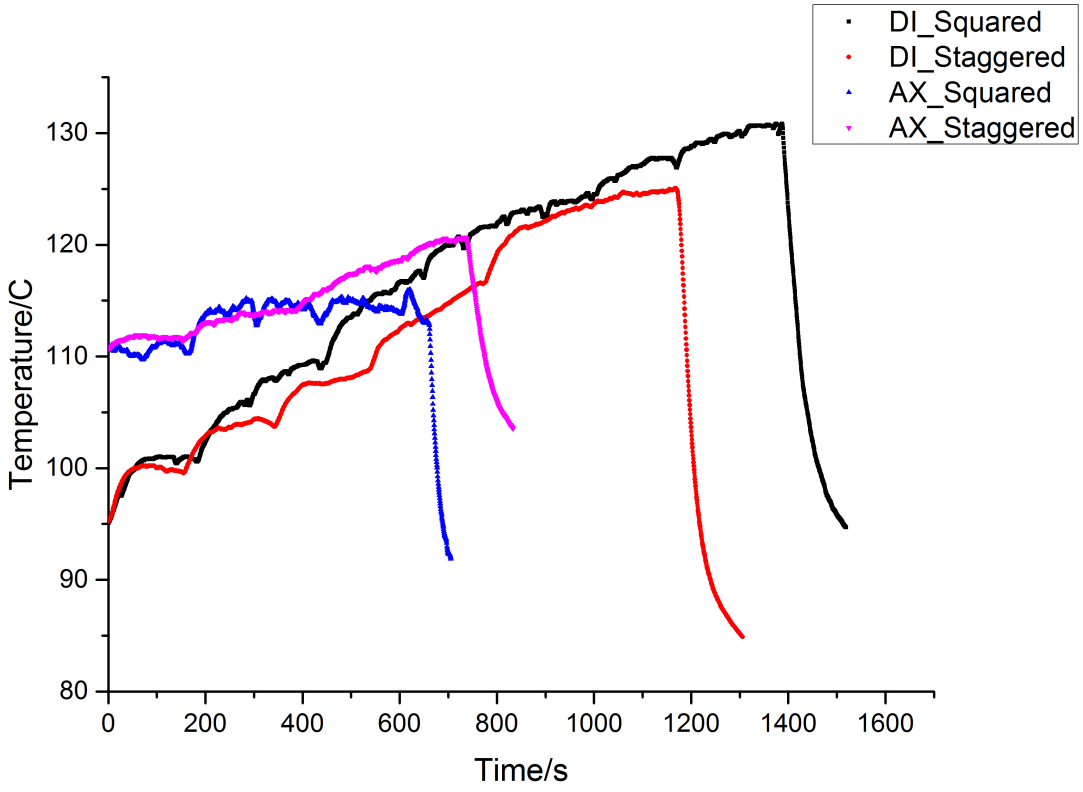

Figure A-10: Temperature measurement of all four on-chip microreactors with different flow configurations and pillar arrangements as a function of time.

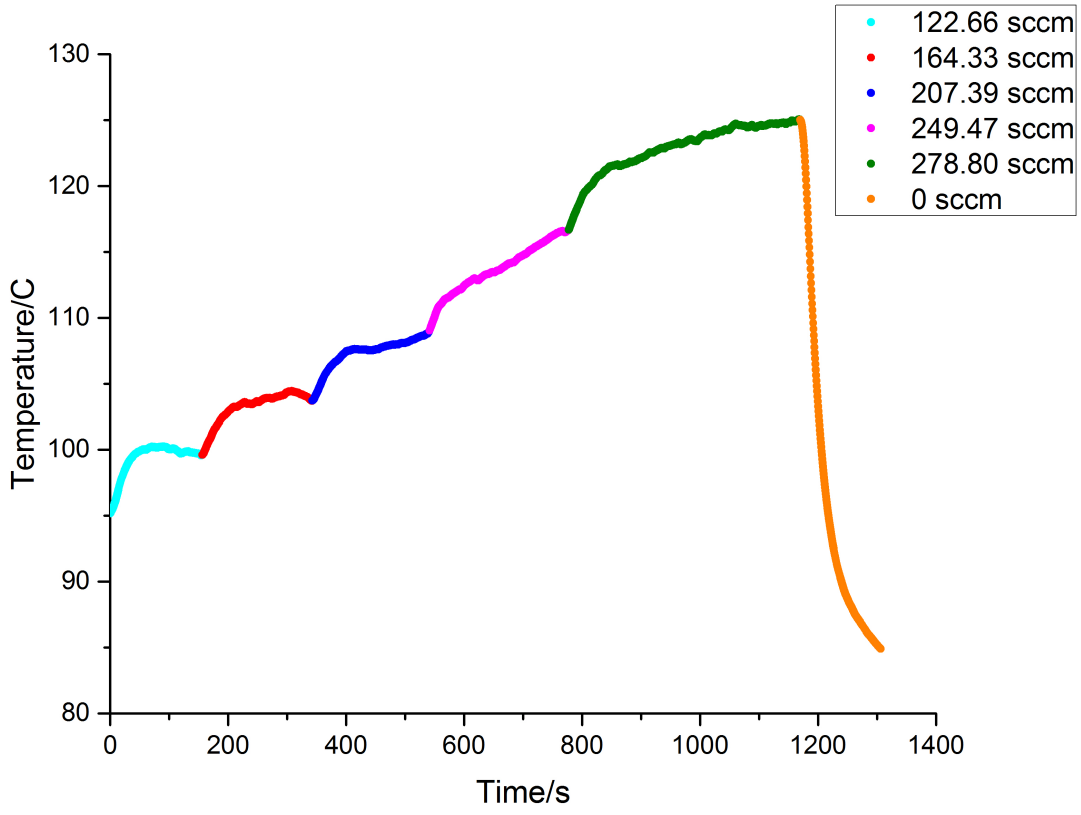

Figure A-11: Raw data of temperature measurement for reactor with staggered pillar arrangement and diagonal flow configuration.